AD-A082 357 BATTELLE COLUMBUS LABS OH F/G 20/6
OPTICAL WAVEGUIDE SCATTERING REDUCTION.(U)
JUN 79 D W VAHEY F33615-78-C-1426
UNCLASSIFIED AFAL -TR-79-1113 NL

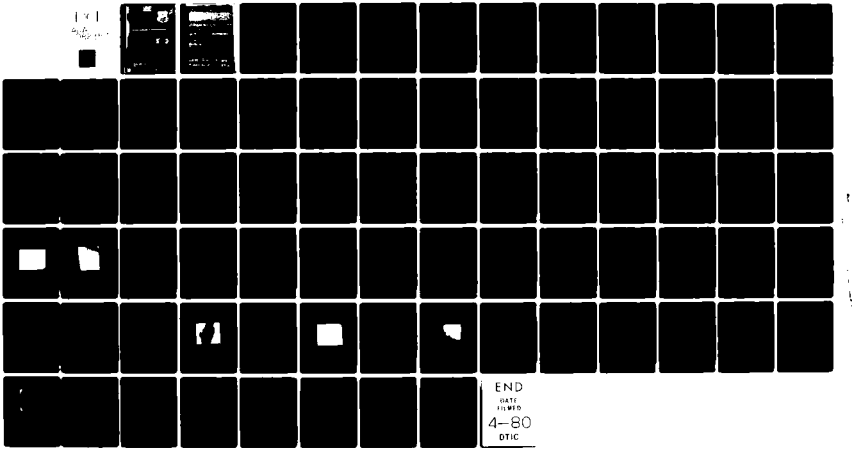

END
DATE FILMED
4-80
DTIC

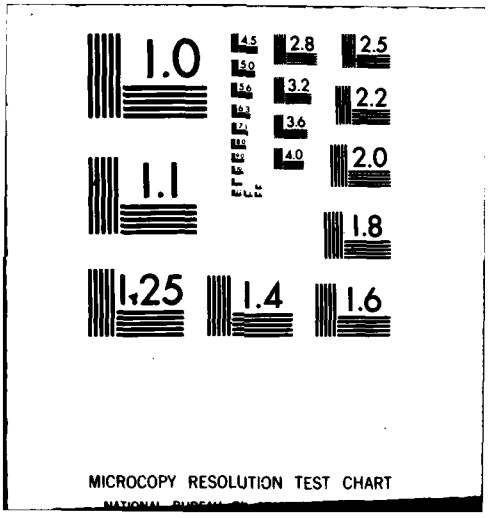
1.0
1.1
1.25
1.4
1.6
1.8
2.0
2.2
2.5
2.8
3.2
3.6
4.0
4.5
5.0
5.6
MICROCOPY RESOLUTION TEST CHART

SECURITY CLASSIFICATION OF THIS PAGE *(When Data Entered)*

REPORT DOCUMENTATION PAGE

READ INSTRUCTIONS BEFORE COMPLETING FORM

1. REPORT NUMBER: AFAL-TR-79-1113	2. GOVT ACCESSION NO.
3. RECIPIENT'S CATALOG NUMBER	
4. TITLE *(and Subtitle)*: Optical Waveguide Scattering Reduction	5. TYPE OF REPORT & PERIOD COVERED: Final - 4/15/78 - 4/15/79
	6. PERFORMING ORG. REPORT NUMBER
7. AUTHOR(s): David W. Vahey	8. CONTRACT OR GRANT NUMBER(s): F33615-78-C-1426
9. PERFORMING ORGANIZATION NAME AND ADDRESS: Battelle Columbus Laboratories, 505 King Avenue, Columbus, Ohio 43201	10. PROGRAM ELEMENT, PROJECT, TASK AREA & WORK UNIT NUMBERS: P.E. 62204F, 2001 02 61
11. CONTROLLING OFFICE NAME AND ADDRESS: Avionics Laboratory (AFWAL/AADO), Air Force Wright Aeronautical Laboratories, Wright-Patterson AFB, OH 45433	12. REPORT DATE: June 1979
	13. NUMBER OF PAGES: 64
14. MONITORING AGENCY NAME & ADDRESS *(if different from Controlling Office)*: Final rept. 15 Apr 78 - 15 Apr 79	15. SECURITY CLASS. *(of this report)*: Unclassified
	15a. DECLASSIFICATION/DOWNGRADING SCHEDULE

16. DISTRIBUTION STATEMENT *(of this Report)*

Approved for public release; distribution unlimited.

17. DISTRIBUTION STATEMENT *(of the abstract entered in Block 20, if different from Report)*

18. SUPPLEMENTARY NOTES

19. KEY WORDS *(Continue on reverse side if necessary and identify by block number)*

Integrated Optics, Optical Waveguides, Scattering, Scattering Reduction, In-Plane Scattering, Out-of-Plane Scattering, Anisotropic Scattering, Surface Roughness, Microdomains, Phase Transformations, Optical Polishing, Ti Films, Ti Diffusion, Diffusion Conditions, $LiNbO_3$, Electrooptic Effect, Photorefractive Effect, Scattering Theory, Surface Contamination, Ion Exchange

20. ABSTRACT *(Continue on reverse side if necessary and identify by block number)*

The goal of this program was the reduction of scattering in optical waveguides to levels commensurate with the required preformance characteristics of an integrated optical acoustooptic spectrum analyzer. Waveguides formed by thermal diffusion of Ti films into $LiNbO_3$ substrates were emphasized. The best waveguides were obtained by diffusing thin ($\leq$ 280 Å) Ti films or by polishing waveguides made from thicker films to reduce surface contamination believed to be associated with Li-Ti-O compound formation. Residual scattering in the best

DD FORM 1 JAN 73 1473 EDITION OF 1 NOV 65 IS OBSOLETE

SECURITY CLASSIFICATION OF THIS PAGE *(When Data Entered)*

401011

waveguides is found to be strongly anisotropic and polarization dependent. Additionally, it can be enhanced by an applied electric field, but not by the photorefractive generation of optical damage using a beam propagating parallel to the optical axis. Possible sources of residual scattering that were considered are antiphase microdomains, separated crystalline phases, and diffused-film imperfections. None of these could be definitely identified as the source of residual scattering in good Ti:$LiNbO_3$ waveguides; however, only the microdomains hypothesis appears to be ruled out on the basis of its conflicts with various data.

Theoretical understanding of the scattering process was extended during the program to account for the two-and three-dimensional nature of waveguide scatterers, and to account for volume as well as surface-roughness scattering centers. The main prediction of the theory is that surface roughness dominates out-of-plane scattering while volume imperfections dominate in-plane scattering. This prediction was verified experimentally. However, the dependence of scattering on optical wavelength predicted by the theory was in conflict with preliminary experimental observations.

FOREWORD

This is the final technical report on research performed at Battelle Columbus Laboratories under Air Force Contract #F33615-78-C-1426 under Project FY1175-78-31129. It describes work performed during the period April 15, 1978, to April 15, 1979. The author's final draft was submitted June 8, 1979, and the revised final report was submitted November 15, 1979. The Principal Investigator was Dr. David W. Vahey. The Air Force Project Engineer was Dr. Douglas Wille of the Air Force Avionics Laboratory.

This work was carried out with active support from all members of the Battelle Optical Sciences Group, including especially Nile Hartman, Carl Verber, Charles Chapman, Richard Pugh, Van Wood and Richard Kenan.

The active participation and interest on the part of Air Force Project Engineer Douglas Wille did much to shape the course of the research. The open lines of communication that he established with frequent on-site visits helped to provide a close sponsor-contractor working relationship that was most beneficial to the program, and for which the author is extremely grateful.

TABLE OF CONTENTS

TABLE OF CONTENTS
(Continued)

LIST OF ILLUSTRATIONS

LIST OF ILLUSTRATIONS
(Continued)

I. INTRODUCTION

Over the past several years a number of schemes have been devised for performing useful optical signal processing functions in an integrated optics format.[1,2] One of the most attractive of these is an acoustooptic spectrum analyzer[1] now being developed under Air Force sponsorship. In the device a waveguided beam is Bragg-diffracted by a surface acoustic wave. The diffracted beam is focused by a lens on a detector array, where there exists a one-to-one correspondence between the element in the array that is illuminated and the oscillation frequency of the surface acoustic wave.

One problem yet impeding the development of a versatile spectrum analyzer is optical waveguide scattering. Owing to the propagation of the processing beam parallel to and just beneath the waveguide surface, scattering centers associated with surface roughness and defects in the top one micron of material have a devastating effect on the information content of a guided wave. This is true even for surfaces and materials of such high quality that a beam traveling normal to the surface is perturbed by an almost immeasurable amount.

An example showing the deleterious effects of optical waveguide scattering on spectrum analyzer performance is that in which two closely spaced frequencies are simultaneously present on the surface acoustic wave, one of them in much greater strength than the other. In this event, scattered light from the stronger diffracted-beam component can arrive at the same detector element as the unscattered weaker diffracted beam-component. The weaker signal will be partially or totally masked. The effect is one that limits the dynamic range of the system. To avoid the problem, small-angle in-plane waveguide scattering must be reduced in intensity to the point where other sources of spurious signal, such as those resulting from lens aberrations and positioning errors, dominate. As integrated optics component technology improves, increasing emphasis will be placed on the need for reducing waveguide scattering to the lowest possible levels. This has been the goal of the present program.

In this report we describe experimental and theoretical approaches used toward reaching this goal, as well as insight that these approaches have provided regarding the physical nature of the scattering mechanism. Waveguides formed by Ti diffusion into $LiNbO_3$ substrates have been emphasized, since these are the current waveguides of choice for the spectrum-analyzer application.

However, many of the methods and procedures are applicable to other types of waveguides, including thin-film waveguides sputtered on SiO_2-Si substrates.

The achievements of the program reported here include the following:

- A theoretical analysis of both in-plane and out-of-plane scattering that extends the work of Marcuse[3] and Boyd and Anderson[4];
- A modulation technique for studying weak out-of-plane scattering in the presence of scattering from non-waveguide sources;
- A 50 dB dynamic range system for studying in-plane scattering;
- Controlled polishing techniques for removing scattering material at or near the surface of an optical waveguide;
- Demonstration of the utility of Nomarski microscopy for examining the surface of optical waveguides and substrates;
- Acquisition of in-plane scattering data at several visible wavelengths;
- Development of novel diagnostic methods for obtaining information about sources of scattering, including methods based on electrooptic, photorefractive, and superstrate refractive-index effects.

These achievements have enabled us to draw the following conclusions regarding the nature of scattering in Ti-diffused $LiNbO_3$ waveguides:

- Bulk scattering, at least some of which is diffusion-induced, is far more important than surface scattering.
- The bulk scatterers are anisotropic in refractive index and possibly in shape.
- The scatterers are associated with regions that have different electrooptic properties from those of the crystal as a whole.
- Scattering increases in proportion to the amount of Ti used to make the waveguide, but is not, within limits, sensitive to the time and temperature of the diffusion treatment.
- Scattering is similar for x-cut and y-cut crystals.

The recipe that we employ for our best waveguides requires the use of thin 150 Å-300 Å Ti layers diffused for 3 h at 950°C in flowing O_2, followed by a rapid quench to 600°C and a slow cool to room temperature. For waveguides formed using thicker Ti films, some improvement in quality is always obtained by lightly polishing the finished waveguide, even when all Ti has been diffused into the surface.

The above recipe applies for waveguides used with beam propagation perpendicular to the c-axis. For the parallel configuration, however, our best low scattering performance was obtained using a thick Ti film (about 720 Å) and a long post-fabrication polish—long enough, in fact, to remove most of the initially formed waveguide layer.

II. THEORY OF OPTICAL WAVEGUIDE SCATTERING

Most of the data presented in this report show the angular distribution of light scattered from an initially collimated waveguided beam. Since individual scattering imperfections are not observed, only indirect information about their nature is available. The accuracy and extent of this information depends on the realism of physical models used to describe scatterers and on the completeness of the theory employed to correlate scattering data with these models. Accordingly, considerable effort has been expended on theoretical aspects of the waveguide scattering problem, the results of which are described in this section.

Two approaches to the problem are characterized as the Green's-function approach and the coupled-mode approach. The former was implemented, for example, by Giallorenzi,[5] and the latter, by Marcuse[3]. When carried out with complete rigor both should give equivalent descriptions of the waveguide scattering problem. It is our belief that the Green's function approach is more suitable for obtaining the scattered energy distribution from an individual imperfection of specified shape. However, if this is not required, the coupled-mode approach is more suitable since it allows for convenient statistical averaging over an ensemble of scattering centers, each of which may be slightly different.

We concentrated on the coupled-mode formalism[3] for two reasons: first, it is mathematically simpler; second, the results are directly applicable to experimental scattered energy distributions.

THE SCALAR WAVE EQUATION

A classic exposition of the coupled-wave formalism as it applied to optical waveguides is found in the book Light Transmission Optics, by Marcuse.[3] He applies the formalism to the particular problem of scattering by surface-roughness fluctuations in symmetric-slab waveguides. The surface roughness is assumed to vary only in the direction of beam propagation. For these reasons, the theory is not directly applicable to $LiNbO_3$ and sputtered thin-film waveguides, which are asymmetric rather than symmetric, and which have volume as well as surface scattering centers that are three

dimensional. Nevertheless, modifications required to generalize Marcuse's results are relatively straightforward. In point of fact, Walter and Houghton extend Marcuse's theory to the case of the asymmetric slab waveguide,[6] and Boyd and Anderson, using heuristic arguments, extended it to include two dimensional scatterers.[4] Our interest is in (1) providing a mathematical basis for the conclusions of Boyd and Anderson[4] and (2) extending the work of all authors mentioned to include the effects of volume scattering centers as well as surface roughness.

The geometry for the calculation is shown in Fig. 1: x is the direction of propagation, z is the axis normal to the waveguide, and θ and ϕ are the polar and azimuthal angles defined in the usual way. For a given power in the (assumed) single waveguide mode, we calculate the out-of-plane power radiated into the solid angle $d\phi d\theta \sin\theta$, as well as the in-plane power scattered into $d\phi$. The electric field amplitude E is governed by the scalar wave equation,

$$E_{xx} + E_{yy} + E_{zz} + k_o^2 N^2(x,y,z)E = 0 \qquad (1)$$

$$N^2(x,y,z) = n^2(z) + \eta(x,y,z)$$

where k_o is the magnitude of the free-space wave vector, N is the total refractive index, n is the refractive index of the unperturbed waveguide, and η is the refractive-index perturbation. We will consider an unperturbed refractive-index profile like that shown in Fig. 2, having substrate index n_2, waveguide index n_1, and superstrate index n_o. We assume that the substrate index n_2 is very close to the guide index n_1. This is a good approximation in $LiNbO_3$ and it greatly simplifies the mathematics.

For bulk scatterers having an average rms index change $|\delta n|$, we model the refractive index variation using the equations

$$\eta(x,y,z) = \eta(z)g(x,y) \qquad (2)$$

$$\eta(z) \simeq 2n_2\delta n \quad z<0$$

$$\eta(z) = 0 \quad z>0$$

That is, the guide index profile is like that indicated by the dashed line in Fig. 2, where the position of the dashed line relative to the unperturbed

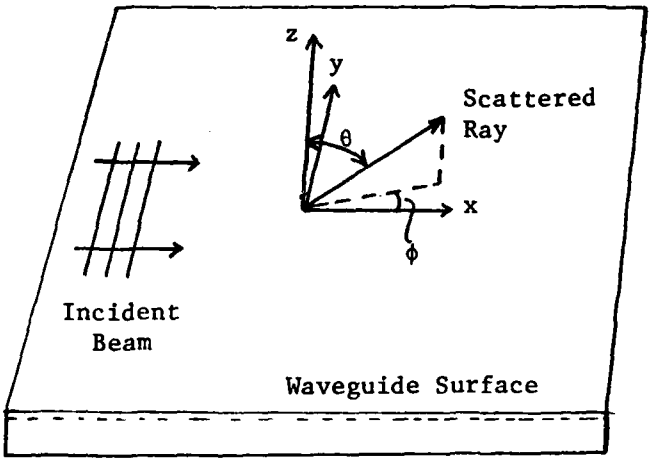

Fig. 1. Geometry for waveguide scattering calculations.

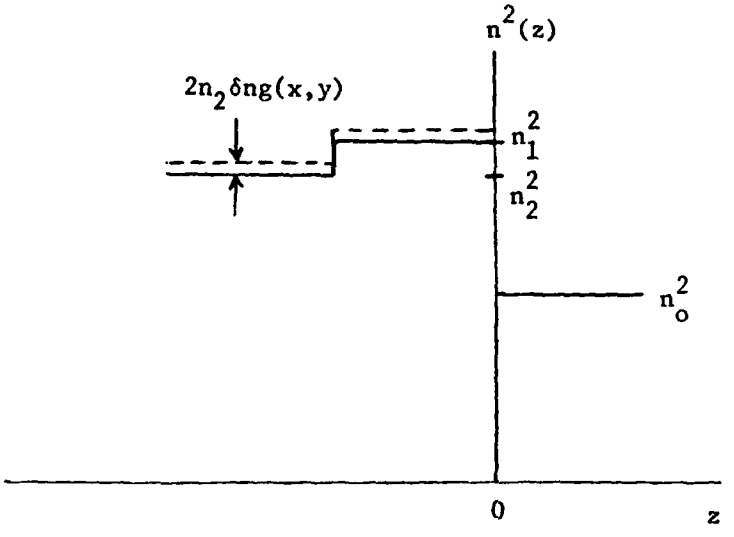

Fig. 2. Refractive-index profiles. Solid line: Unperturbed profile. Dashed line: Profile in the vicinity of a volume scattering center.

solid-line profile varies over the waveguide surface according to the value of $g(x,y)$. By neglecting the z-dependence of δn, we assume that the scattering centers are uniform over depths at least as large as the waveguide mode confinement depth.

For scattering from surface roughness, we follow Marcuse[3] in writing

$$\eta(x,y,z) = (n_1^2 - n_o^2) f(z), \tag{3}$$

$$f(z) = +1 \text{ in } (0<z<\sigma_o g(x,y))$$

$$f(z) = -1 \text{ in } (\sigma_o g(x,y)<z<0)$$

$$f(z) = 0 \text{ elsewhere}$$

where σ_o is the rms surface roughness.

For both surface and volume scattering centers, the random function $g(x,y)$ describes the spatial distribution of scattering centers over the waveguide surface. At any point (x,y) the value $g(x,y)$ indicates either the index perturbation, relative to δn, or the surface height perturbation, relative to σ_o. Thus, $g(x_o,y_o) = 0$ means that there is no perturbations at point (x_o,y_o), while $g(x_o,y_o) = 1$ means that the perturbation has its rms average value at (x_o,y_o).

SOLVING THE SCALAR WAVE EQUATION

A solution to the scalar wave equation, Eq. (1), is obtained by expanding the electric field in terms of the discrete guided modes and the continuum of radiation modes. The single discrete mode of the waveguide we are considering has a spatial variation of the electric field that may be written $E_o(z)e^{i\underline{\beta}_o \cdot \underline{r}}$, where $E_o(z)$ is the modal amplitude distribution normal to the waveguide plane, $\underline{\beta}_o = \beta_o(\cos\phi, \sin\phi, 0)$ is the wavevector, and $\underline{r} = (x,y,0)$ is the position.

Each element of the continuum of radiation modes has a field distribution that may be similarly written $E(\rho,z)e^{i\underline{\beta}\cdot\underline{r}}$, where $E(\rho,z)$ is the modal amplitude variation of the radiation mode characterized by the continuous parameter ρ, and $\underline{\beta}$ is the wavevector analogous to the guided mode wavevector

that describes the variation of phase of the radiation mode in the waveguide plane. Each radiation mode is described by a real value of $\rho = (k_o^2 n_2^2 - \beta^2)^{1/2}$ in accord with Maxwell's equations and appropriate boundary conditions. Derivation of the forms of $E_o(z)$ and $E(\rho,z)$ are given in Ref. (3) for symmetric waveguides and in Ref. (5) for asymmetric waveguides. Also presented in these references are the orthogonality relationships satisfied by the various discrete and radiation modes, which we will later have occasion to employ. In particular, we note

$$P_{rad}\delta(\rho-\rho') = \beta/2\omega\mu_o \int_{-\infty}^{\infty} E(\rho,z)E^*(\rho',z)dz \tag{4}$$

$$0 = \beta_o/2\omega\mu_o \int_{-\infty}^{\infty} E_o(z)E^*(\rho,z)dz$$

$$P = \beta_o/2\omega\mu_o \int_{-\infty}^{\infty} |E_o(z)|^2 dz$$

In these expressions, P_{rad} is the power in the radiation field contained within an infinitesimal range of the parameter ρ, and P is the power in the waveguide mode. Both powers are given for beams of unit width.

In the case of weak scattering of an initially guided beam propagating in the x-direction, we may define scattering functions $c_o(\phi,x)$ and $q(\rho,\phi,x)$ that describe the amplitude of the field scattered at an angle ϕ into the guided and radiation modes, respectively. In terms of these functions, the total field may be written

$$E(x,y,z) \simeq E_o(z)e^{i\beta_o x} + \int_o^{2\pi} d\phi c_o(\phi,x)E_o(z)e^{i\underline{\beta}_o(\phi)\cdot\underline{r}} \tag{5}$$

$$+ \int_o^{2\pi} d\phi \int_o^{\infty} d\rho\ q(\rho,\phi,x)E(\rho,z)e^{i\underline{\beta}(\phi)\cdot\underline{r}} \quad ,$$

$$\underline{\beta}_o(\phi) = \beta_o(\cos\phi,\sin\phi,0) \quad ,$$

$$\underline{\beta}(\phi) = (k_o^2 n_2^2 - \rho^2)^{1/2}\ (\cos\phi,\sin\phi,0) \quad ,$$

$$\underline{r} = (x,y,0)$$

The quantities c_o and q are determined by inserting Eq. (5) into Eq. (1) and making use of the orthogonality conditions given in Eq. (4). If, for example, both sides of the equation obtained by inserting Eq. (5) into Eq. (1) are multiplied by $E_o(z)e^{-i\underline{\beta}_o(\phi')\cdot r}$ and the resulting expressions are integrated over z,y, and ϕ, we obtain

$$0 \simeq (2\pi/\beta_o|\cos\phi'|) \int_o^x dx'[c_o''(\phi',x') + 2i\beta_o\cos\phi'\ c_o'(\phi',x')] + k_o^2\ \eta_o\ G(\phi',x)$$

$$G(\phi',x) = \int_o^x dx' \int_{\substack{\text{beam} \\ \text{width } W}} dy'g(x',y')e^{i\beta_o x - i\underline{\beta}_o(\phi')\cdot\underline{r}} \quad . \tag{6}$$

The term η_o is defined as the part of the integral $(\beta_o/2\omega\mu_o P) \int_{-\infty}^{\infty} dz\ \eta(x,y,z)|E_o(z)|^2$ that is proportional to g(x,y). Thus, η_o depends on the model for scattering center employed.

A result similar to Eq. (6) is found for the radiation-mode amplitude q when we insert Eq. (5) into Eq. (1), premultiply both sides by $E(\rho',z)e^{-i\underline{\beta}_r(\phi')\cdot\underline{r}}$, and integrate over z,y,ϕ and ρ. The result can be written using Eq. (6) by making the substitutions

$$c_o(\phi',x') \rightarrow q(\rho',\phi',x) \quad , \tag{7}$$

$$\underline{\beta}_o(\phi') \rightarrow \underline{\beta}(\phi')$$

and by redefining η_o to mean the part of the expression $(\beta/2\omega\mu_o P_{rad}) \int_{-\infty}^{\infty} dzE^*(\rho',z)E_o(z)\eta(x,y,z)$ proportional to g(x,y).

Equation (6) for c_o or its counterpart for q are most simply treated by assuming that the functions c_o and q change slowly enough that their second derivatives may be neglected. Then, following Marcuse[3], we consider forward(+) and backward(-) traveling waves satisfying the boundary conditions

$$c_o^{(+)}(\phi',0) = 0 = q^{(+)}(\rho',\phi',0) \quad , \tag{8}$$

$$c^{(-)}(\phi',L) = 0 = q^{(-)}(\rho',\phi',L) \quad ,$$

where L is the length of the scattering medium, measured in the direction of propagation. The slowly-varying solutions to the coupled-wave equations that satisfy these boundary conditions are simply

$$c_o^{(+)}(\phi,L) = c_o^{(-)}(\phi,0) = -k_o^2(\eta_o)_{in}G(\phi,L)/4\pi i \tag{9}$$

$$q^{(+)}(\rho,\phi,L) = q^{(-)}(\rho,\phi,0) = -k_o^2(\eta_o)_{out}G(\rho,\phi,L)/4\pi i.$$

We have introduced the modified notation $(\eta_o)_{in}$ and $(\eta_o)_{out}$ to call attention to the different expressions that apply for in-plane and out-of-plane scattering. Additionally, note that in the usual case which the dimensions of the scattering area are much larger than those of the scatterer, both $G(\phi,L)$ and $G(\rho,\phi,L)$ can be replaced by a single Fourier-transform

$$G(\underline{K}(\phi)) = \int_{-\infty}^{\infty}\int_{-\infty}^{\infty} dxdy\ g(x,y)e^{i\underline{K}(\phi)\cdot\underline{r}} \quad , \tag{10}$$

where $\underline{K}(\phi) = \beta_o(1,0,0) - \beta_o(\cos\phi,\sin\phi,0)$ for in-plane scattering or $\underline{K}(\phi) = \beta_o(1,0,0) - \beta(\cos\phi,\sin\phi,0)$ for out-of-plane scattering. That is, $\underline{K}(\phi)$ is the scattering vector.

Let us consider a scattering area that consists of N scattering centers located at $\underline{r} = \underline{r}_i$, i = 1,2,..N. With $\underline{q}_i = \underline{r}-\underline{r}_i$, we may write

$$g(x,y) = \sum_{i=1}^{N} \gamma_i(q_{1i},q_{2i}) \tag{11}$$

where γ_i describes the scattering perturbation in the vicinity of the i th scattering center. The widths Δq_{1i} and Δq_{2i} over which γ_i is significantly different from zero describes the size of the scattering centers. Inserting Eq. (11) into Eq. (10), we find

$$G(\underline{K}) = \sum_{i=1}^{N} e^{i\underline{K}\cdot\underline{r}_i}\int_{-\infty}^{\infty}\int_{-\infty}^{\infty} d\underline{q}_i\gamma_i(\underline{q}_i)e^{i\underline{K}\cdot\underline{q}_i} \tag{12}$$

For identical scatterers having a width $\underline{a}$ in the x direction and b in the y direction, we find

$$G(\underline{K}) = \sum_{i=1}^{N} e^{i\underline{K}\cdot\underline{r}_i} \, ab \, \mathrm{sinc}(K_x a/2\pi)\mathrm{sinc}(K_y b/2\pi) \tag{13}$$

CALCULATIONS OF SCATTERED POWER

The amount of power scattered in the plane of the waveguide into a range of angles $d\phi$ centered at ϕ is calculated from the formula

$$dP_{in}(\phi) = P(2\pi/\beta_o)\, c(\phi,L)c^*(\phi,L)d\phi \quad , \tag{14}$$

where P is the initial power per unit width of the beam in the waveguide. Similarly, the light scattered out of plane into a range of angles $d\phi$ centered at ϕ and into a range of radiation modes $d\rho$ centered at ρ is

$$d^2P_{out}(\rho,\phi) = P_{rad}(2\pi/\beta)q(\rho,\phi,L)q^*(\rho,\phi,L)d\rho d\phi. \tag{15}$$

By way of Eq. (9) part of the angular dependence of each of these expressions depends on the factor $|G|^2$. For identical, randomly positioned scatterers,

$$|G|^2 = a^2b^2\mathrm{sinc}^2(K_x a/2\pi)\mathrm{sinc}^2(K_y b/2\pi) \sum_{i,j=1}^{N} e^{i\underline{K}\cdot(\underline{r}_i-\underline{r}_j)}. \tag{16}$$

For scattering angles such that $|\underline{K}(\phi)|^{-1}$ is comparable to sample dimensions, the sum in Eq. (16) has the value N^2. Otherwise, it fluctuates about the average value N and we have

$$|G|^2 = Na^2b^2\mathrm{sinc}^2(K_x a/2\pi)\mathrm{sinc}^2(K_y b/2\pi). \tag{17}$$

From another point of view, that in which the scattering distribution is a random function g(x,y), having correlation lengths a and b in the x and y directions, respectively, the evaluation of $|G|^2$ is performed using methods discussed in Ref. (3). The result is similar to that of Eq. (17), and is

$$|G|^2 = 4\, Na^2b^2\, L(K_x a)L(k_y b) \tag{18}$$

where

$$L(q) = (1 + q^2)^{-1} \tag{19}$$

is the Lorentzian function.

Despite the differences in models employed in the calculations, Eqs. (17) and (18) for $|G|^2$ show rather similar behavior. We will write

$$|G|^2 = 4Na^2b^2H(\phi) \tag{20}$$

to separate the model-dependent angular variation of scattering from the dependence on scattering center size and number. From Eq. (18), which we will use to be specific,

$$H(\phi) \rightarrow H_o(\phi) = [1 + \beta_o{}^2a^2(1-\cos\phi)^2]^{-1}\ [1 + \beta_o{}^2b^2\sin^2\phi]^{-1} \tag{21}$$

for in-plane scattering, while

$$H(\phi) \rightarrow H(\rho,\phi) = [1 + (\beta_o - \beta\cos\phi)^2a^2]^{-1}[1 + \beta^2b^2\sin^2\phi]^{-1} \tag{22}$$

for out-of-plane scattering.

In-Plane Scattering

The next step in the evaluation of scattered power is the calculation of the perturbation terms η_o. These are different for in- and out-of-plane scattering and for volume and surface-roughness scattering. For in-plane scattering we find from the definitions stated below Eqs. (6) and (7)

$$(\eta_o)_{in} = 2n_2\delta n \quad \text{(volume scattering)}, \tag{23}$$

$$(\eta_o)_{in} = (n_1^2 - n_o^2)\sigma_o E_o^2(0)(\beta_o/2\omega\mu_o P) \quad \text{(surface roughness scattering)}.$$

Since neither of these expressions depends on ϕ, the angular distribution of scattered energy for in-plane scattering is that of the function $H_o(\phi)$ alone. Therefore it is not possible to differentiate between surface and volume scattering on the basis of the angular distribution of scattered light. However, the dependence of $(n_o)_{in}$ on the field at the surface $E_o(0)$ for scattering from surface roughness shows that the strength of scattering from this source depends on the modal characteristics of the waveguide. This is not true for volume scattering, at least to the extent that the scatterers extend well into the substrate,as our model assumes.

For a single-mode waveguide operating just above cutoff, an approximate expression for the square of the electric field at the surface is

$$E_o^2(0) \simeq (4\omega\mu_o P/\beta_o D)(n_1^2 - n_2^2)(n_1^2 - n_o^2)^{-1} \quad . \tag{24}$$

The square of the field reduces to about 60% of this value for a strong single-mode waveguide, operating just below the onset of the second mode. By combining Eqs. (9),(14),(20),(21),(23), and (24), we find the in-plane distribution of scattered power to be

$$[dP_{in}(\phi)]_{surf} = d\phi P(4\pi^2/n_1)(Na^2b^2\sigma_o^2/D^4\lambda_o)(n_1^2-n_2^2)H_o(\phi) \tag{25}$$

For volume scatterers, the corresponding formula is

$$[dP_{in}(\phi)]_{vol} = d\phi P(16\pi^2 n_2^2/n_1)(Na^2b^2\delta n^2/\lambda_o^3)H_o(\phi) \quad . \tag{26}$$

The differential in-plane scattering cross section is defined by the expression

$$\sigma_{in}(\phi) = (dP_{in}/d\phi)/PWL, \tag{27}$$

and is equal to

$$[\sigma_{in}(\phi)]_{surf} = (4\pi^2/n_1)(\Sigma a^2 b^2 \sigma_o^2/D^4\lambda_o)(n_1^2-n_2^2)H_o(\phi) \quad , \tag{28}$$

$$[\sigma_{in}(\phi)]_{vol} = (16\pi^2 n_2^2/n_1)(\Sigma \delta n^2 a^2 b^2/\lambda_o^3)H_o(\phi) \quad ,$$

where $\Sigma = N/LW$ is the surface density of scattering centers. For scattering centers of comparable size and density in $LiNbO_3$, we have the ratio

$$[\sigma_{in}]_{vol}/[\sigma_{in}]_{surf} = 440(D^4\delta n^2/\lambda_o^2\sigma_o^2)$$

Taking $D = 2$ μm, $\lambda_o = 0.633$ μm, $\sigma_o = 10^{-2}$ μm, and $\delta n = 10^{-2}$, we find that volume scattering centers are 18000 times as effective as surface roughness for causing in-plane scattering.

Out-of-Plane Scattering

The out-of-plane scattered-energy distribution is calculated from the results of Eqs. (9), (15), (20) and (22). It is, however, first necessary to obtain expressions for the perturbation term $(\eta_o)_{out}$ that appears in Eq. (9). The definition of $(\eta_o)_{out}$ from the discussion below Eqs. (6) and (7) is

$$(\eta_o)_{out} = (\beta/2\omega\mu_o P_{rad})I(\rho) \quad , \tag{29}$$

$$g(x,y)\ I(\rho) = \int_{-\infty}^{\infty} dz E^*(\rho,z)\eta(x,y,z)E_o(z) \quad .$$

For volume scattering centers, $\eta = 2n_2\delta n g(x,y)$ in the substrate and $\eta = 0$ in the superstrate. The last part of Eq. (29) becomes

$$I(\rho)_{vol} = +\ 2n_2\delta n \int_{-\infty}^{0} E^*(\rho,z)E_o(z)dz. \tag{30}$$

Most of the contribution to this integral comes from the waveguide layer $-D \leq z \leq 0$. In this region $E_o(z) \sim \cos(\pi z/D + \pi/2)$ for a well-confined

single guided mode, while $E(\rho,z) \sim \cos[(k_o^2 n_1^2 - k_o^2 n_2^2 + \rho^2)^{1/2}(z + d/2)]$ for even radiation modes. For large values of ρ, the integrand of Eq. (30) is rapidly oscillating in the region of interest, and $I(\rho)_{vol}$ is small. This result indicates that scattering from guided modes tends to populate radiation modes with small values of ρ. These are modes that have plane-wave components that propagate in the substrate at small angles to the incident beam, and decay exponentially in the superstrate. Using the orthogonality between guided and radiation modes, Eq. (30) may be rewritten

$$I(\rho)_{vol} = -2n_2 \, \delta n \int_o^\infty E^*(\rho,z) E_o(z) dz \quad , \tag{31}$$

where the integral is carried out over the superstrate. For the case $\rho << k_o n_2$ and $n_2 \simeq n_1$, both guided and radiation modes have decay constants close to $k_o(n_1^2 - n_o^2)^{1/2}$. The result of integrating Eq. (31) is then

$$I_{vol} \simeq -n_2 \delta n E^*(\rho,0) E_o(0) / k_o (n_1^2 - n_o^2)^{1/2} \quad . \tag{32}$$

For scattering from surface roughness, the perturbation of Eq. (3) is to be inserted in Eq. (29), with the result

$$I_{surf} = (n_1^2 - n_o^2) \sigma_o E^*(\rho,0) E_o(0). \tag{33}$$

Both expressions are seen to depend on the value of the fields at the surface. An approximate value of $E_o^2(0)$ is given in Eq. (24). Marcuse[18] derives an expression for $E^*(\rho,0)$ which we approximate as

$$E^2(\rho,0) \simeq (4\omega\mu_o P_{rad}/\pi\beta)\rho^2/k_o{}^2(n_1^2-n_o^2). \tag{34}$$

By combining Eqs. (9),(15),(20),(22),(29), and (32-34), we obtain the differential scattered power

$$\frac{d^2P}{d\phi d\rho} = (4/\pi n_1)(Na^2b^2/\lambda_o)(D_{pert}^2/D)(n_1^2-n_2^2)(n_1^2-n_o^2)^{-2}\rho^2 H(\rho,\phi)P \tag{35}$$

$$D_{pert} = n_2\delta n/k_o(n_1^2-n_o^2)^{1/2} \quad \text{(volume scattering)}$$

$$D_{pert} = (n_1^2-n_o^2)\sigma_o \quad \text{(surface-roughness scattering)},$$

The radiation mode label ρ is related to the scattering angle θ of Fig. 1 according to

$$\rho = k_o n_2 \cos\theta. \tag{36}$$

This permits us to recast Eq. (35) in the more common format of a differential scattering cross section, $\sigma_{out} = d^2P/d\Omega^2/PWL$. We find

$$\sigma_{out} = (32\pi^2 n_2^2)(\Sigma a^2b^2/\lambda_o^4)(D_{pert}^2/D)(n_1^2-n_2^2)(n_1^2-n_o^2)^{-2}\cos^2\theta H(\theta,\phi), \tag{37}$$

$$H(\theta,\phi) = [1 + k_o^2 n_2^2 a^2(1-\sin\theta\cos\phi)^2]^{-1}[1 + k_o^2 n_2^2 b^2 \sin^2\theta\sin^2\phi]^{-1}$$

where $\Sigma = N/WL$ is the surface density of scattering centers.

For scattering centers of comparable size and density in $LiNbO_3$, we have the ratio

$$[\sigma_{out}]_{vol}/[\sigma_{out}]_{surf} \simeq (0.1)\ \delta n^2/k_o^2\sigma_o^2 \tag{38}$$

Taking $k_o = 10\ \mu m^{-1}$ $\sigma_o = 10^{-2}$ μm and $\delta n \simeq 10^{-2}$, we find that surface scatterers are 1000 times as effective as volume scatterers in producing forward,

out-of-plane scattering into the substrate. This is opposite to the situation that we found to exist in the case of in-plane scattering, where volume scattering centers exerted the dominant effect.

Waveguide Attenuation

A theoretical expression for the waveguide attenuation coefficient is found by integrating the differential scattering cross section $\sigma_{out}(\theta,\phi)$ over all solid angles in the substrate. A graphical analysis of the integral suggests that the dominant contribution comes from the angular range

$$-\cos\theta \lesssim (k_o n_2 a)^{-1/2} \tag{39}$$

$$|\sin\phi| \lesssim (k_o n_2 b)^{-1}$$

We will crudely evaluate the integral by setting $H(\theta,\phi) = 1$ in this angular range and $H(\theta,\phi) = 0$ elsewhere. This should at least give us the correct dependences of attenuation on the parameters $k_o n_2 a$ and $k_o n_2 b$. We find

$$\alpha_{surf} = (4/3)(2/\pi)^{1/2} n_2^{-1/2} (n_1^2 - n^2{}_2)(\Sigma a^{1/2} b \sigma_o^2 / \lambda_o^{3/2} D) \quad , \tag{40}$$

$$\alpha_{vol} = (1/3\pi^2)(2/\pi)^{1/2} n_2^{3/2} (n_1^2 - n_2^2)(\Sigma a^{1/2} b \lambda_o^{1/2} / D)(n_1^2 - n_o^2)^{-3}$$

for the attenuation coefficients associated with surface and volume scattering centers, respectively.

Using the Theory to Describe Experimental Data

Although Eq. (40) may be applied directly to the analysis of experimental attenuation data, Eq. (28) for the in-plane scattered-energy distribution must be extended to account for the method usually employed to take in-plane scattering data. This method is illustrated by Fig. 3 on page 21. Light scattered over a range of angles is projected by a lens onto a slit of width s. If the focal length of the lens is f and the index of the waveguide mode is approximately n_1, the range of angles observed is

$$\Delta\phi = s/n_1 f \quad , \tag{41}$$

where $\Delta\phi$ is measured in the waveguide medium. The scattered power incident on the detector is

$$\Delta P = PWL\sigma_{in}(\phi)s/n_1 f \tag{42}$$

This power is referenced to the power incident on the detector when the unscattered beam is projected onto the slit. This power is

$$P_{max} = PW^2 s/f\lambda_o \tag{43}$$

The in-plane scattered-energy-distribution function is the ratio

$$\frac{\Delta P}{P_{max}} = (L\lambda_o/n_1 W)\sigma_{in}(\phi) \tag{44}$$

For the case of scattering by volume imperfections, we find using the second of Eqs. (28),

$$\Delta P/P_{max} \simeq 16\pi^2(L/W)(\Sigma\delta n^2 a^2 b^2/\lambda_o^2)H_o(\phi) \tag{45}$$

Similar considerations apply to the analysis of out-of-plane scattering data.

The reader interested in more details regarding the coupled mode analysis that has been used to derive the results of this section may find them in Ref. (19)by Marcuse, as well as in Refs. (3) and (18) cited earlier.

III. EXPERIMENTAL APPROACHES TO THE STUDY OF OPTICAL WAVEGUIDE SCATTERING

An ideal situation is that in which sources of scattering are observed directly in nondestructive fashion with sub-micron resolution. The electron microscope is the only instrument we know of with this capability, and even this tool is inadequate when the scatterers constitute a small perturbation of the average environment. Not surprisingly, this is the case with many high-quality waveguide materials. As a result, the major amount of information that can be gathered regarding optical waveguide scattering comes to us through scattered-energy-distribution experiments such as those described in this section. In these experiments, light propagating in a waveguide is scattered and detected as a function of angle or as a function of the position at which scattering occurs, and the measurements are interpreted according to reasonable models to provide indirect information about the nature of scattering sources.

IN-PLANE SCATTERING EXPERIMENTS

Figure 3 shows the experimental configuration used to measure the in-plane scattered energy distribution in Ti:$LiNbO_3$ waveguides. An approximately Gaussian beam is prism-coupled into and out of the waveguide and focused by a simple lens onto a slit coupled to a fiber bundle. The slit is scanned across the focal plane and collects light scattered over an angular range of several degrees about the initial beam direction. When the slit is translated a distance x from the focus, light passed through it to the detector corresponds to light scattered at an angle

$$\phi \simeq x/fn_g \tag{46}$$

in the plane of the waveguide, where f is the focal length of the lens, n_g is the effective index of the waveguide mode, and ϕ corresponds to the angle in the waveguide material.

For the better waveguides we have worked with, the detected signal at n_g $\phi \simeq 1°$ is down 40 dB or more from the peak signal at the focus. A

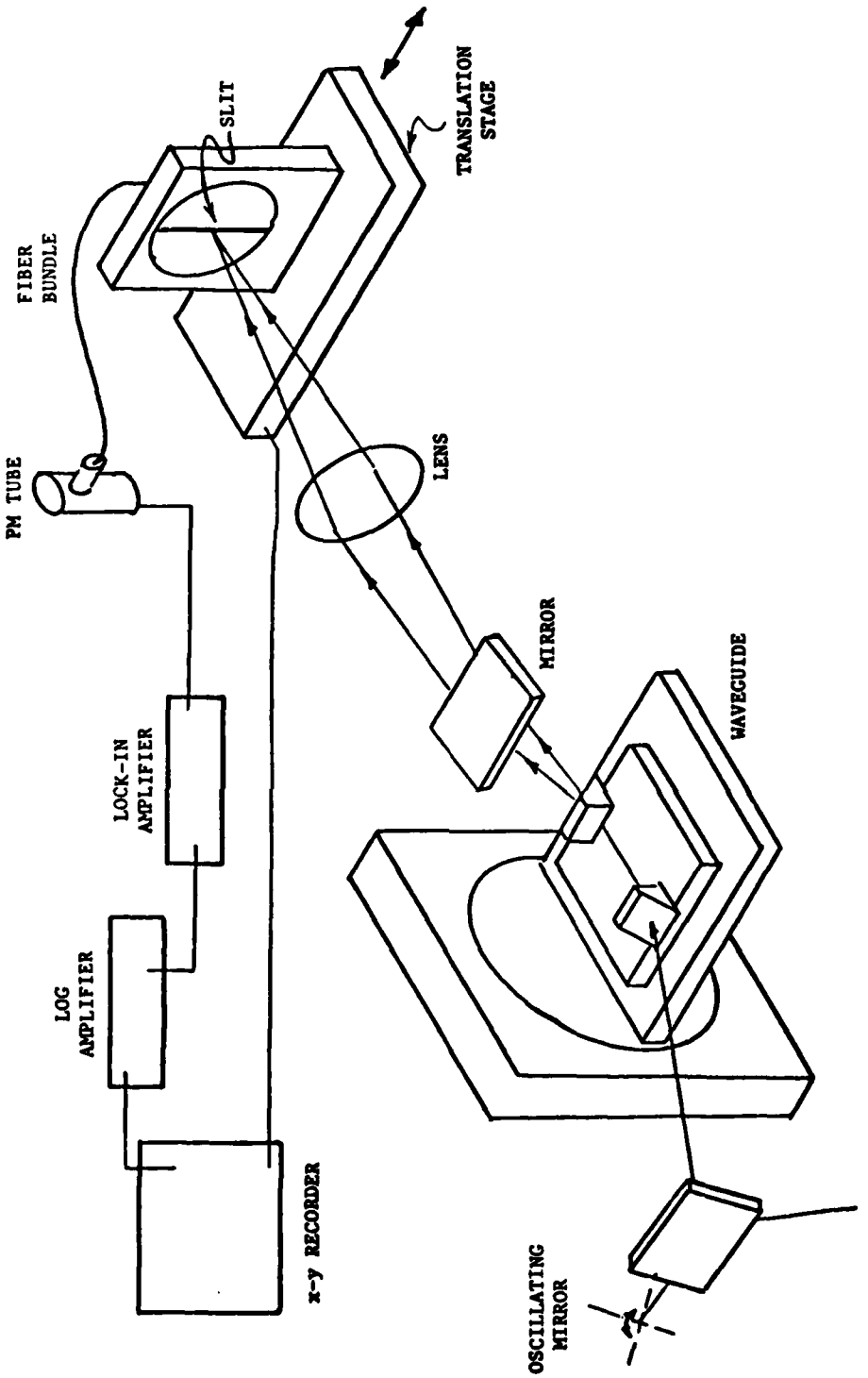

Fig. 3. Experimental configuration for measuring the in-plane scattered-energy distribution.

photomultiplier tube is thus a convenient detector, since it possesses the requisite dynamic range. Our measurements are facilitated by use of a lock-in amplifier operating in a frequency selective mode. The output from the lock-in is converted to logarithmic format by a log-amplifier and displayed using an x-y recorder.

In-plane scattering data are obtained in two steps. First, the lock-in is employed on a high-sensitivity setting to record scattered light levels in a range -30 dB to-50 dB below the peak intensity of the unscattered focused beam. Then the sensitivity of the lock-in is reduced and a scan is made of the intensity profile of the unscattered focused beam.

For the in-plane scattering data presented in this report, the scattered intensity measured in dB reduction from the peak intensity is plotted as a function of the scattering angle measured external to the waveguide, $\phi_{ext} = n_g \phi$. This is a convenience, since n_g varies between 2.2 and 2.3 in our experiments, depending on mode polarization and direction of beam propagation. Interpretation of the data must also be guided by the understanding that the scattered intensity increases linearly with the ratio L/W, where L is the length of the scattering medium, and W is the beam width. In our experiments, L ≈ 18 mm and W ≈ 1.5 mm

In-plane scattering results to be described in Sec. IV were obtained using the system of Fig. 3, with one modification; namely, a mechanical chopper was used in place of the oscillating mirror to modulate the beam. A potential advantage of the oscillating mirror is that light scattered at the input prism is not modulated to the extent that light scattered in the waveguide is and can therefore be rejected at the detector. However, there is still the problem of modulated scattering at the output prism. This constitutes a source of noise that must be evaluated. Early in the program we verified that waveguide scattering dominated over prism scattering in the case of a fairly poor waveguide. Recent evidence suggests that waveguide quality is improved to the level where prism effects can influence the data. At this level it is appropriate to take data with zero input-output prism separation and to subtract the observed scattering distribution from that obtained with a large prism separation. Also data should be taken for several beam locations within the waveguide, and/or several placements of the coupling prisms, and the most representative data used for more detailed analysis. The data presented in

Sec. IV does not for the most part reflect these recommendations. Justification is to be found in the nature of the data and the methods employed to interpret it. First, we avoid quantitative analysis of results which could be in error because of prism-associated scattering. Second, we emphasize changes in the scattered-energy distribution that result from changes in experimental conditions. Prism coupling in and out of the waveguide is a constant of each experiment, and therefore does not, presumably, influence the changes in scattering that are relevant to our analysis.

OUT-OF-PLANE SCATTERING EXPERIMENTS

Early in the program considerable effort was directed toward out-of-plane scattering measurements, particularly the related measurement of waveguide attenuation. The technique that was employed most often is shown in Fig 4. It was thought that the technique offered several advantages over more conventional means for measuring waveguide attenuation, excluding pyroelectric means.[7,8] In any case, a nonpyroelectric method is needed for the study of the out-of-plane scattered-energy distribution in $LiNbO_3$.

In the procedure of Fig. 4 an oscillating mirror is employed to modulate coupling into the waveguide, with the idea that light scattered in the prism will not be similarly modulated and can therefore be rejected at the detector. Second, light scattered into the substrate is studied with the idea that the scattered intensity in the substrate will be greater than in the superstrate, thus affording a signal-to-noise advantage important to the study of very-low-loss waveguides.

We found that light scattered at the prism was not totally modulation free, and that much of it was directed into the substrate where it was necessary to shield it from the fiber bundle. Shielding was also necessary at the output end of the waveguide, whether or not an output coupling prism was employed. The amount of shielding required increases with the substrate thicknesses and refractive index. Thickness is a factor because it constitutes the minimum distance from the prism that shielding can be positioned. Refractive index is a factor because it influences the number of reflections that light undergoes before leaving the substrate and being blocked by the shielding.

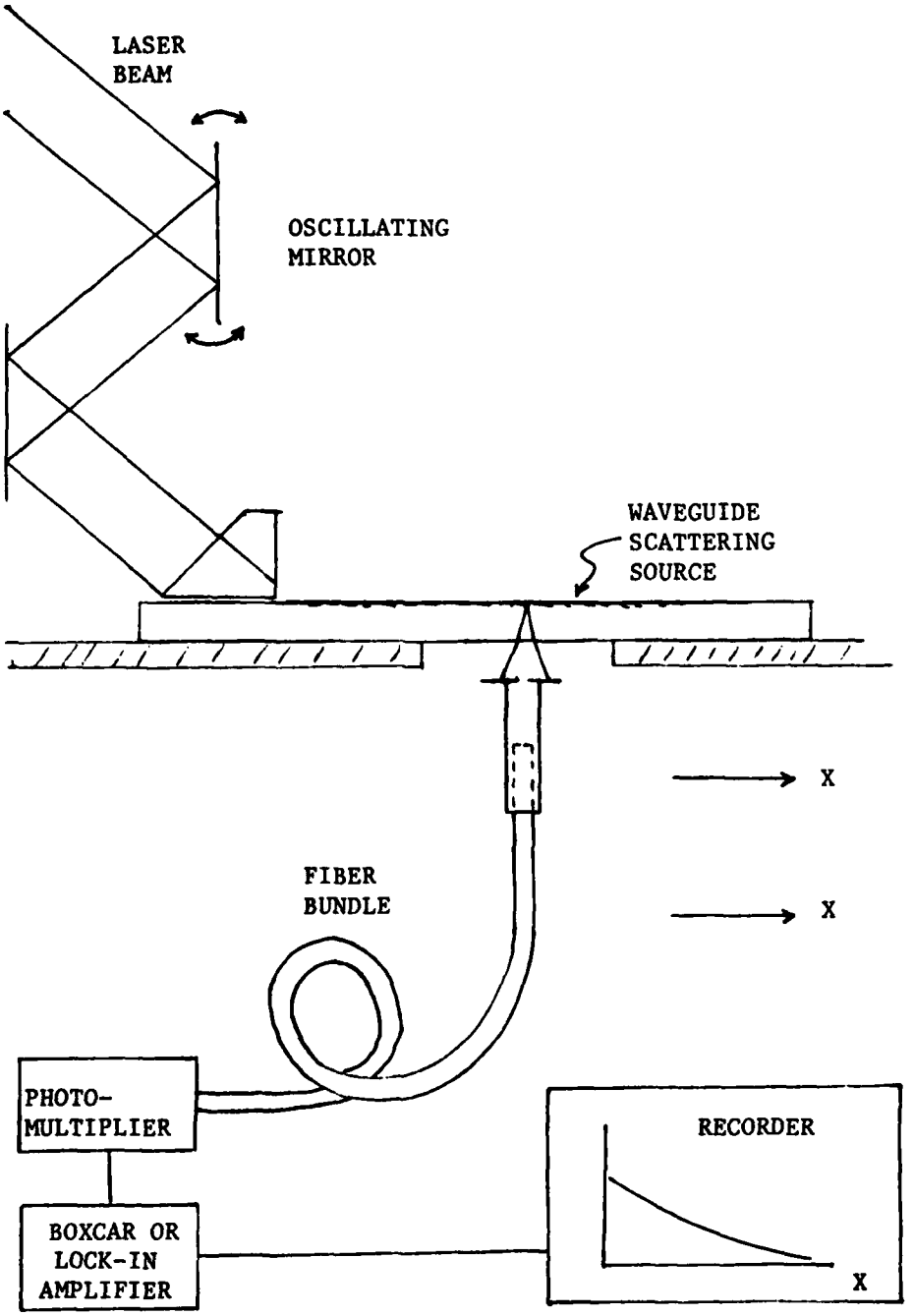

Fig. 4. Experimental configuration for observing out-of-plane waveguide scattering.

The need for shielding reduces the overall length of the waveguide that can be scanned to measure attenuation. This reduces any advantage that may be associated with increased scattered intensity in the substrate region. Consequently, a geometry in which light scattered into the superstrate is detected may, in fact, be superior to the geometry shown in Fig. 4. For the measurement of waveguide attenuation. The geometry of Fig. 4, however, would still be relevant for the study of the out-of-plane scattered energy distribution.

We suspended our measurements in out-of-plane scattering in favor of in-plane measurements that were straightforward to perform and still provided us with a wealth of information. Later in the program, theoretical calculations showed that sources for out-of-plane and in-plane scattering could be very different. In view of the relevance of in-plane scattering to the spectrum-analyzer application, we continued to focus our attention on sources of in-plane scattering for the duration of the program.

IV. IN-PLANE SCATTERING IN Ti:$LiNbO_3$ WAVEGUIDES

In this section we present and interpret in-plane scattering data for various Ti:$LiNbO_3$ waveguides. The data were obtained using the experimental method described in Sec. III. Ti:$LiNbO_3$ waveguides were emphasized for study because they are the current waveguides of choice for the development of an integrated optical spectrum analyzer.[1,9] The data to be presented have led us to the following conclusions regarding the nature of scattering in these waveguides:

(1) Bulk scattering, at least some of which is diffusion-induced, is far more important than surface scattering.

(2) The bulk scatterers are anisotropic in refractive index and possibly in shape.

(3) The scatterers are associated with regions that have different electrooptic properties from those of the crystal as a whole.

(4) Scattering increases in proportion to the amount of Ti used to make the waveguide, but is not, within limits, sensitive to the time and duration of the diffusion treatment.

(5) Scattering is similar for x-cut and y-cut crystals.

The recipe that we employ for our best waveguides requires the use of thin 150 Å-300 Å Ti layers diffused from 3-6 h at 950°C in flowing O_2, followed by a rapid quench to 600°C and a slow cool to room temperature. For waveguides formed using thicker Ti films, some improvement in quality is always obtained by lightly polishing the finished waveguide, even when all Ti has been diffused into the surface.

The above recipe applies for waveguides used with beam propagation perpendicular to the c-axis. For the parallel configuration, however, our best low-scattering performance was obtained using a thick Ti film (about 720 Å) and a long post-fabrication polish—long enough, in fact, to remove most of the initially formed waveguide layer.

IN-PLANE SCATTERING IN A $LiNbO_3$ WAVEGUIDE FORMED USING A 280 Å Ti FILM

The preferred configuration for an RF spectrum analyzer employs TE polarized light propagating nearly perpendicular to the $LiNbO_3$ optic axis. For this configuration we have found the least scattering in waveguides formed using relatively thin Ti films. The data presented here are for a sample obtained by diffusing a 280 Å-thick Ti layer into the substrate for 3 h at 950°C in flowing O_2. However, we have tentative evidence that some small improvement may be obtained by going to even thinner (150 Å) Ti films. The sample we will describe was lightly polished following fabrication to improve its surface condition. This procedure and its benefits will be discussed in detail later.

Figure 5 shows typical in-plane scattered-energy distributions for the TE_o mode for four different directions of beam propagation: 0°, 90°, +45°, and -45° degrees to the optic axis. The anisotropy of the observed scattering strongly suggests that the scattering mechanism is not surface roughness. (The surface polish of the initial substrate was an "optical" polish provided by the supplier using proprietary methods). The anisotropy could result from volume inhomogeneities that, as seen by the waveguided beam, are not simply circular in shape. Or the anisotropy could result from circular scattering centers having an anisotropic refractive index. Alternatively, both geometric and refractive-index anisotropies could be relevant.

Figure 6 shows the scattered energy distribution for the same waveguide when the TM_o mode is propagated at the same four angles to the optical axis. The variation with angle is similar to that for TE_o modes in the case of propagation parallel and perpendicular to the optic axis. However, TM_o mode scattering is least at $\pm$ 45° to the optic axis, while TE_o mode scattering is greatest in these directions.

This behavior is difficult to explain if the scattering centers are assumed to have an isotropic refractive index and an anisotropic shape. For example, rod-like scatterers with their long axis at 90° to $\underline{c}$ could be proposed to explain the data taken for propagation parallel and perpendicular to the optic axis. However, scattering at $\pm$ 45° would then be expected to be intermediate to that at 0° and 90°, in contrast to what we observe.

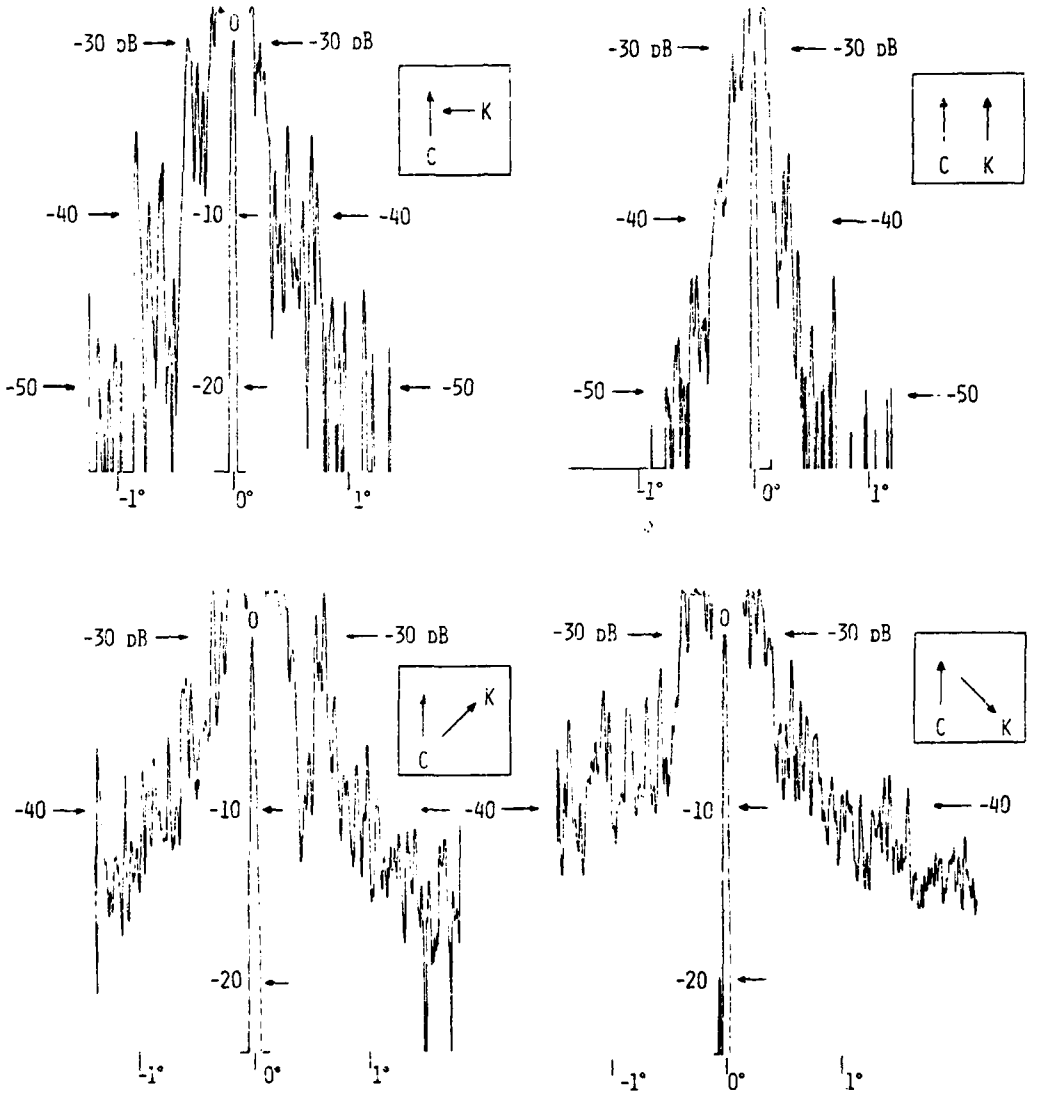

Fig. 5. In-plane scattered energy distributions for four different directions of TE_o mode propagation.

(NOTE: The position of the arrowhead of the c-axis was not deemed to be experimentally significant, and could be opposite that shown by the insets).

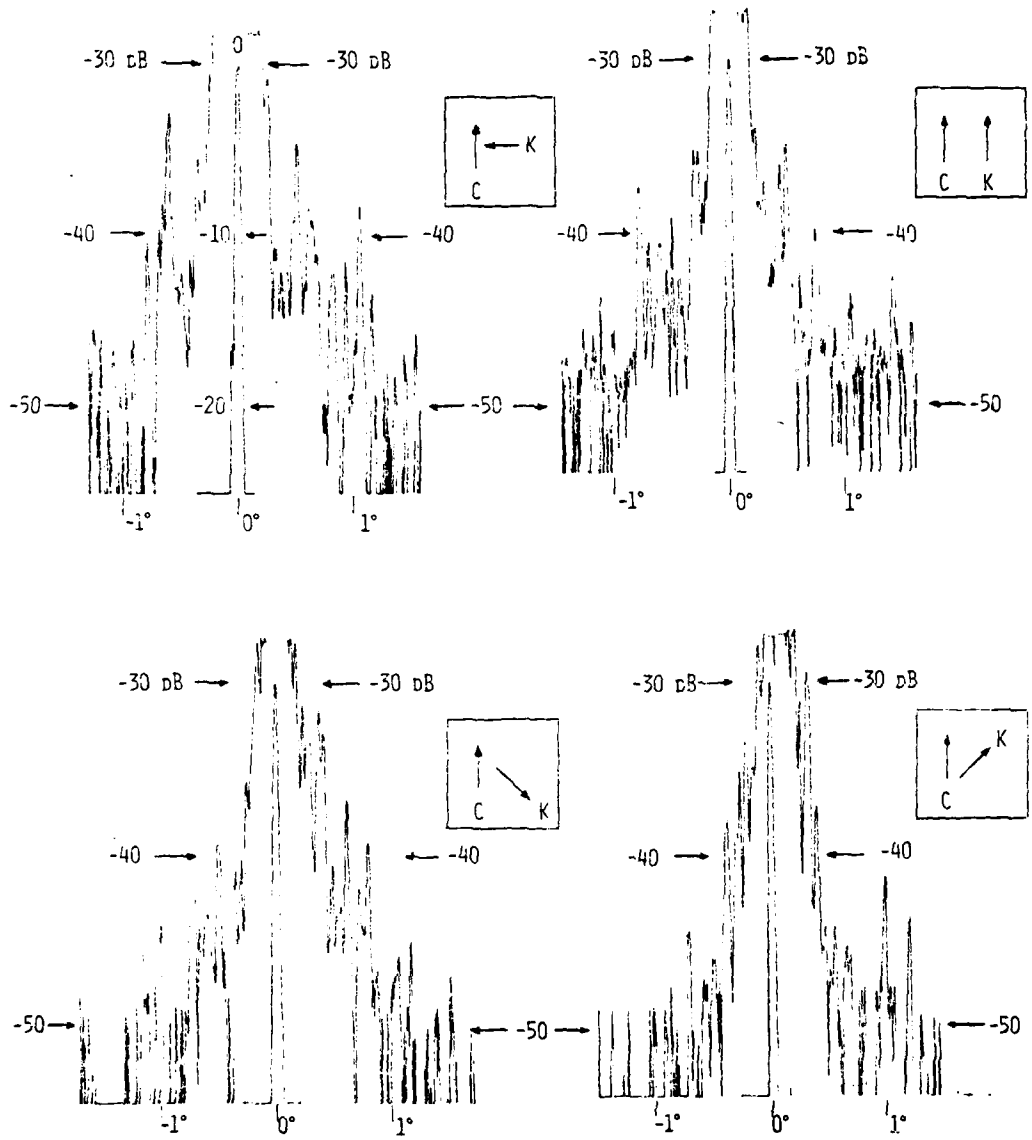

Fig. 6. In-plane scattered energy distributions for four different directions of TM_o mode propagation.

(NOTE: The position of the arrowhead of the c-axis was not deemed to be experimentally significant, and could be opposite that shown by the insets).

More likely is the possibility that the scattering centers exhibit an anisotropic refractive index variation. Regions where the crystal stoichiometry fluctuates or where crystalline compounds containing Ti are formed during diffusion are possible examples of such anisotropic scattering centers. The simple process of Ti diffusion is known to produce anisotropic index changes, even in the absence of compound formation, because of the tendency of the Ti to occupy well defined lattice sites.[10]

IN-PLANE SCATTERING IN A $LiNbO_3$ WAVEGUIDE FORMED USING A 720 Å Ti FILM

The Surface Contamination Layer

We have observed considerably greater scattering than seen in Figs. 5 and 6 in the case of $LiNbO_3$ waveguides formed using thicker Ti films. A quantitative indication of the variation of waveguide quality with Ti-film thickness is shown by the graph of Fig. 7. Increased scattering is associated with the increase in a granular "orange peel" layer found on the surface of the sample after Ti diffusion. Figure 8 shows an example of this granular layer, taken using differential interference contrast (Nomarski) microscopy. The demarkation between the granular diffused region and an adjacent undiffused region is readily apparent. Observation of the demarkation using an interference microscope suggests that the thickness of the granular layer is a few hundred Angstroms; i.e., comparable to the thickness of the diffused metal film. The characteristic lateral dimension of the granular structure is about one micron. The features seen in Fig. 8 are roughly characteristic of all waveguides we have formed using a Ti-film thickness of 720 Å. For thinner films, the granular structure is much less apparent, but still present. Fig. 9 shows the surface texture obtained in an extreme case, that of a 26 h diffusion of a 1000 Å-thick Ti film. The granular structure is approximately two microns in size. We emphasize that the structure is not undiffused TiO_2, but rather is associated with the diffused species.

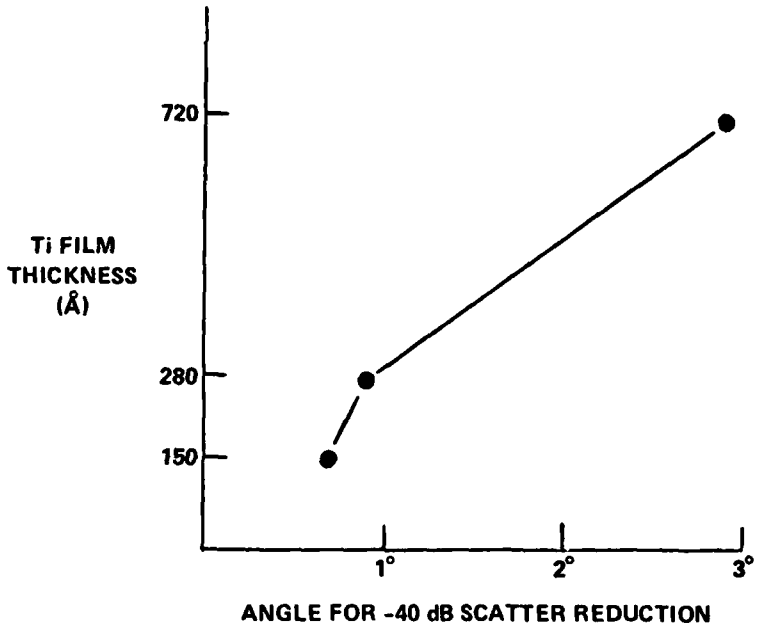

Fig. 7. Dependence of scattering on Ti film thickness.

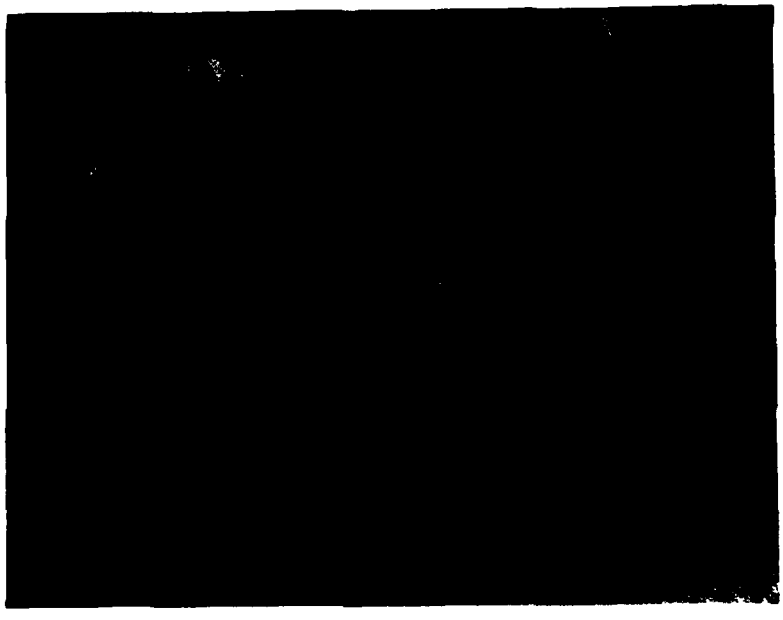

Fig. 8. Nomarski micrograph showing the granular surface texture associated with Ti diffusion (750 Å Ti film, 3 h diffusion, 500X magnification). Vertical line shows the demarkation between the diffused region (right) and the undiffused region (left).

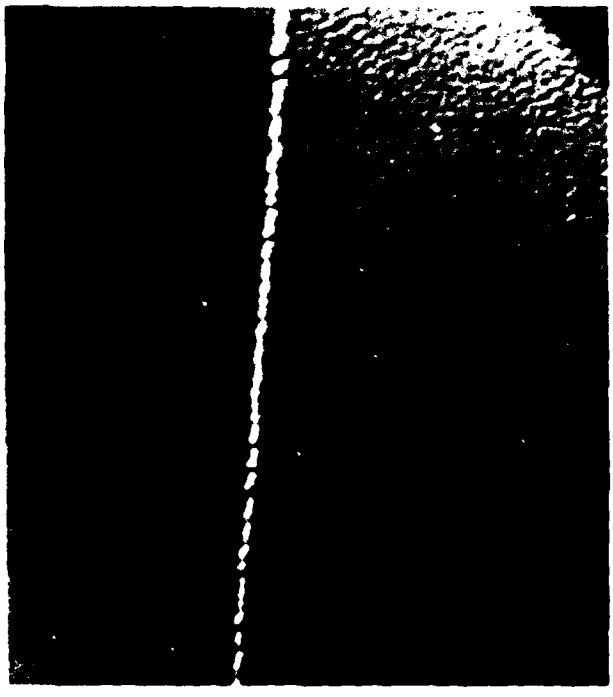

Fig. 9. Nomarski micrograph showing the granular surface texture associated with Ti diffusion (1000 Å Ti film, 26 h diffusion, 500X magnification). Vertical line shows the demarkation between the diffused region (right) and the undiffused region (left).

Waveguide Improvement by Post-Diffusion Polishing

It is not surprising that diffusion of the metal increases the volume of the crystal; however, we can only speculate as to why a nonuniform surface profile results. Burns et al [11] have obtained evidence of higher than anticipated Ti concentration within the top 0.3 μm of diffused $LiNbO_3$ waveguides having an overall depth of several microns. They tentatively ascribe this to the formation of Li-Ti-O compounds such as $Li_2Ti_3O_7$. Perhaps the granularity we observe is evidence of the formation of crystallites of this material. The crystallites would presumably have an index considerably different from that of $LiNbO_3$, and so would be efficient volume scattering centers. In corroboration of this expectation we find sometimes considerable reduction in waveguide scattering by polishing the waveguide surface. The polishing is performed after diffusion using a colloidal suspension of silica (trade name: Syton) in conjunction with a microcloth lap. The polishing is done by applying several pounds per square inch pressure to the sample as it moves about the circumference of a vibrating table. Polishing continues for at least a time long enough to remove the granular "orange peel" structure on the surface. In our experiments, this was 45-90 minutes. Polishing for this length of time does not appear to significantly alter the modal properties of the waveguide.

We have found continued scattering reduction in waveguides formed using 720 Å Ti films when we continue to polish the waveguide surface for times well in excess of those required simply to remove the granularity. However, for waveguides formed using 280 Å Ti films, there appears to be no advantage to extra polishing once the granularity is removed. And for 150 Å films, where the granularity is barely visible, there may be no advantage to any post-diffusion polishing.

Figure 10 and 11 show the dramatic improvement in waveguide quality that can result from long polishing of samples formed using thick Ti films. The waveguide employed in the experiment was fabricated by diffusing 720 Å of Ti into the y-cut surface for 3 h at 950°C in flowing O_2, followed by a rapid quench to 600°C. The data show the typical peak scattering level in the waveguide, measured at an external angle of 1°, as a function of total

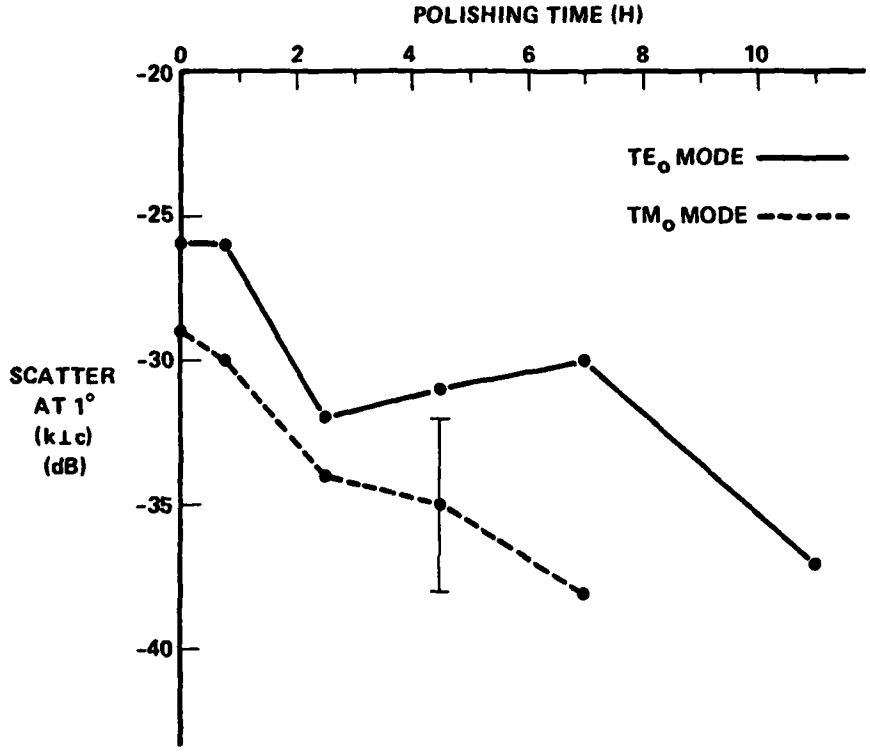

Fig. 10. Dependence of scattering on post-fabrication polishing of a waveguide formed using a 720 Å Ti film. TE_o and TM_o modes propagating perpendicular to the optic axis are shown.

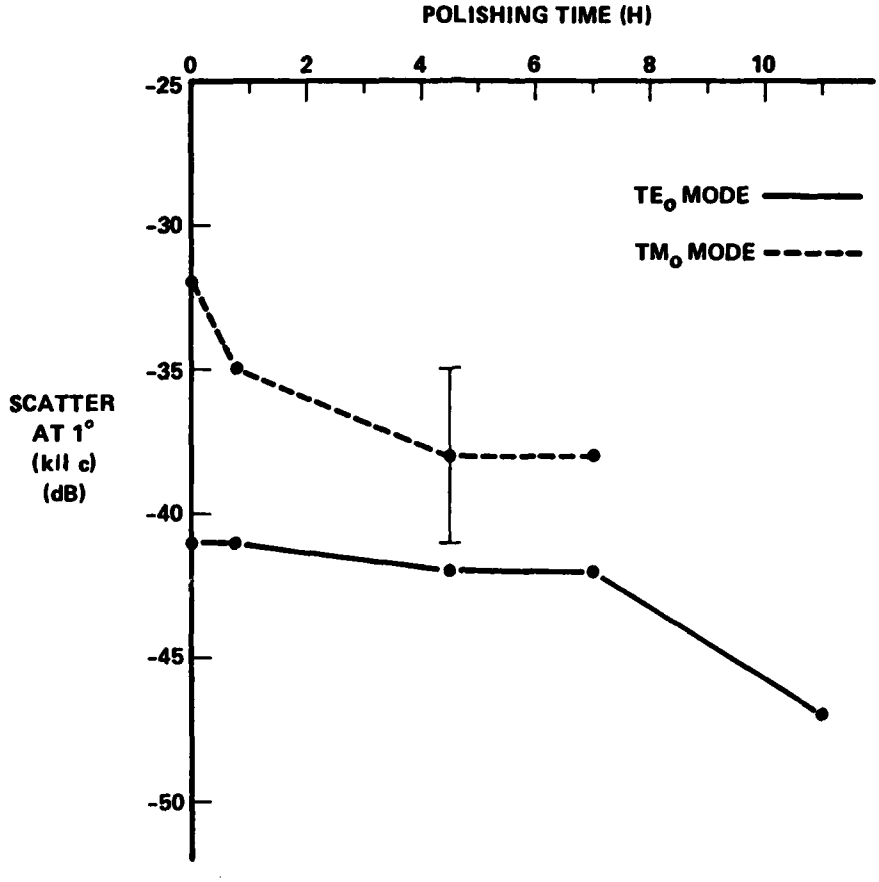

Fig. 11. Dependence of scattering on post-fabrication polishing of a waveguide formed using a 720 Å Ti film. TE_0 and TM_0 modes propagating parallel to the optic axis are shown.

polishing time. Data for the case of propagation perpendicular and parallel to the optic axis are presented in Figs. 10 and 11 respectively. Through 7 h polishing, there is monotonic reduction in scattering of TM modes, while TE modes remain essentially static. Perhaps this reflects a greater sensitivity of TM modes to surface conditions, owing to the larger value of the electric field at the surface for these modes.

After 7 h polishing, the scattering levels for the three modes that propagate as ordinary waves (TE_o, $\underline{k} \parallel \underline{c}$; TM_o, $\underline{k} \parallel \underline{c}$; and TM_o, $\underline{k} \perp \underline{c}$) are comparable and significantly less than the scattering level for the one mode that propagates as an extraordinary wave (TE_o, $k \perp c$). This suggests that the scatterers could have an anisotropic refractive index, and share the same symmetry axis as the host crystal. It is also requisite that the scatters be roughly isotropic in shape; that is, roughly circular when viewed in the plane of the waveguide, if this model is to apply.

After 11 h total polishing, a dramatic reduction in scattering level of TE_o modes is shown by the data. (Unfortunately, TM_o modes were not examined). Scattering for the case of propagation parallel to the optic axis remains 10 dB lower than scattering for the case of propagation perpendicular to the optic axis, but both experiments show 6-7 dB reduction in scattering level resulting from the additional 4 h polishing. A possible interpretation is that the Ti-rich surface contamination layer suggested by the data of Burns et al [11] has been completely polished away, leaving a superior waveguide.

Figure 12 shows the scattered-energy distribution for the case TE_o, $\underline{k} \parallel \underline{c}$, 11 h polish, which is the best waveguide scattering performance we have obtained to date. The performance of the same waveguide when used for propagation perpendicular to the optic axis, however, was no better than that shown in Fig. 5, for a waveguide which was formed with a 280 Å Ti film, and which did not have extensive post-diffusion polishing.

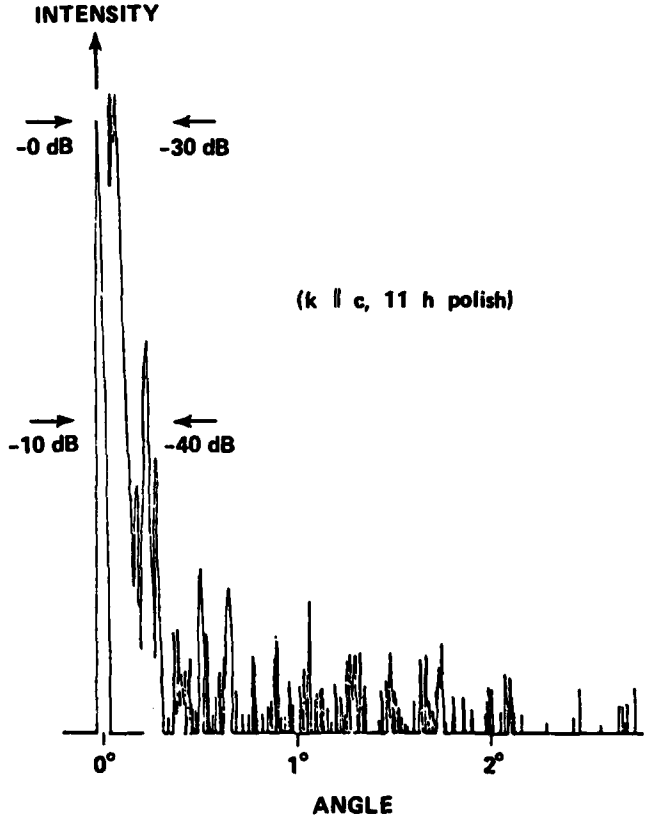

Fig. 12. In-plane scattered-energy distribution for the TE_0 mode propagating parallel to the optic axis, after 11 h total polishing time.

V. POSSIBLE SOURCES OF RESIDUAL SCATTERING IN Ti:$LiNbO_3$ WAVEGUIDES

As Sec. IV has shown, near surface scattering tentatively identified with Li-Ti-O compound formation is a potentially significant source of scattering in Ti:$LiNbO_3$ waveguides.[11] Nevertheless, it is not the only source of scattering. We have considered several possible sources for the residual scattering in Ti:$LiNbO_3$ waveguides that is not eliminated through the use of low Ti concentrations or post-diffusion polishing. These include (1) localized occurrence of the phase transformation $LiNbO_3 \rightarrow LiNb_3O_8$;[12] (2) Ti-free regions resulting from local imperfections in the diffused film; and (3) occurrence of microscopic antiphase domains (microdomains), which are regions of crystalline imperfection characterized by c-axis reversal.[13] A fourth possible source of the observed anisotropic scattering in $LiNbO_3$ is anisotropic surface roughness associated with the uniaxial crystalline nature of the material. While this is a candidate worthy of study in the future, we have, during the program, considered only the first three candidate scattering mechanisms, and these to varying degrees. We present our results in this section. Emphasis is placed on the possible occurrence of antiphase microdomains, since this scattering mechanism was given the greatest attention and provided the most intriguing experimental results.

ANTIPHASE MICRODOMAINS AND ELECTRIC-FIELD INFLUENCE ON SCATTERING

Etching studies by Ohnishi[13] have shown that domain reversal can occur at the surface of $LiNbO_3$ upon heating at the high temperatures required to make waveguides. In unheated samples, reversed domains were found to be needle-like structures having a diameter of less than 1 μm and a length typically 300 μm, lying parallel to the c-axis. We have found similar effects upon etching $LiNbO_3$ samples, however, the observation of propagation-direction-dependent scattering in $LiNbO_3$ waveguides first led us to suspect antiphase microdomains as a scattering mechanism, owing to their cylindrical shape. Later we considered that the cylindrical structures seen after etching were oriented in the wrong direction to result in increased scattering for

propagation perpendicular to the c-axis, as we had observed. Nevertheless, by the time of this consideration we had obtained positive indication of an electric-field dependent component of scattering that increased the attractiveness of the microdomain hypothesis.

Electric-Field Dependent Scattering in Ti:$LiNbO_3$ Waveguide

The experiment that we performed is indicated schematically in Fig. 13a. Silver-paste electrodes were applied to the surface of a good quality waveguide, about 1-mm apart. Light was prism-coupled into and out of the waveguide and propagated in the gap region. The in-plane scattering distribution was measured with 500 V and 0 V applied. The results of the experiment are shown in Figs. 14 and 15. An electric field applied parallel to the optic axis is seen to result in a significant increase in waveguide scattering (20 dB at 1°). The scattering decreases when the applied field is removed. The magnitude of the effect appears to be independent of the polarity of the applied voltage.

Figure 13b shows how this observation may be interpreted using the microdomain hypothesis. In the absence of an applied field, the index of the microdomain is close to that of its surroundings and minimum scattering occurs. In the presence of an applied field an electrooptic index change $\Delta n = 0.5\, n_e^3 r_{33} E_o$ is induced in the crystal. Owing to c-axis reversal in the microdomain, the sign of the index change in that region is opposite to that in the host crystal. The optical beam therefore sees a net index change of $|\delta n| = 2|\Delta n|$ localized in the vicinity of the microdomain. The sign of δn depends on the polarity of the applied voltage; however, scattering from the induced index change goes as δn^2 and is polarity independent.

Photorefractive Effects on Waveguide Scattering

As a further test of the microdomain hypothesis, we attempted to generate a similar scattering effect to that shown in Fig. 14 using the photorefractive properties of $LiNbO_3$. In this experiment, a beam of wavelength 515 nm was propagated for a period of time in Ti:$LiNbO_3$ sample 109. The

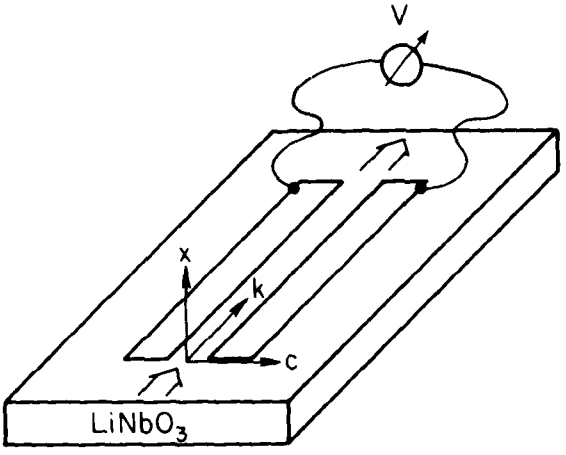

Fig. 13(a). Waveguide geometry for observing electric-field dependence of scattering.

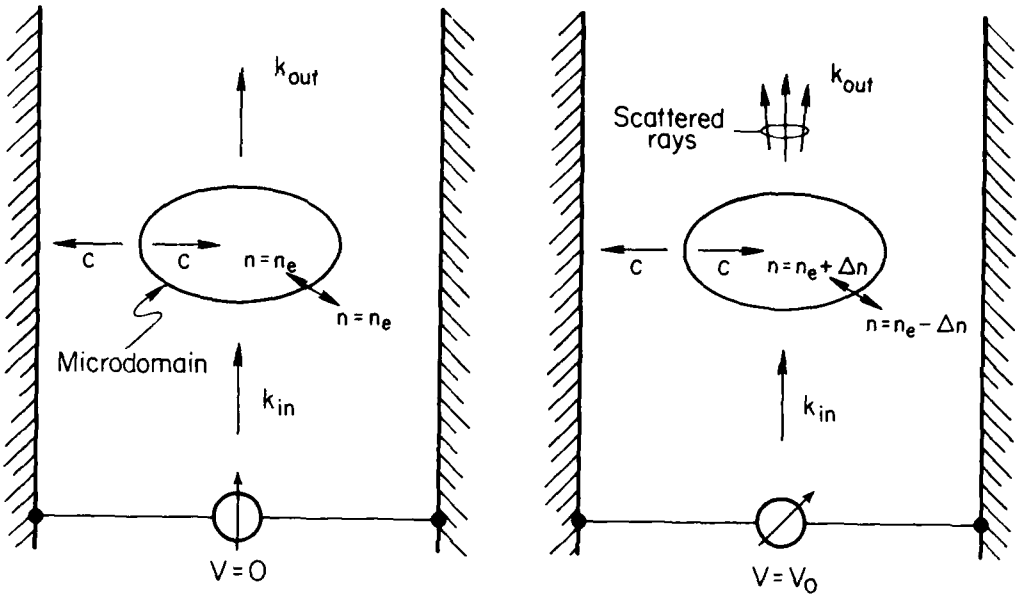

Fig. 13(b). Microdomain model for voltage-induced scattering.

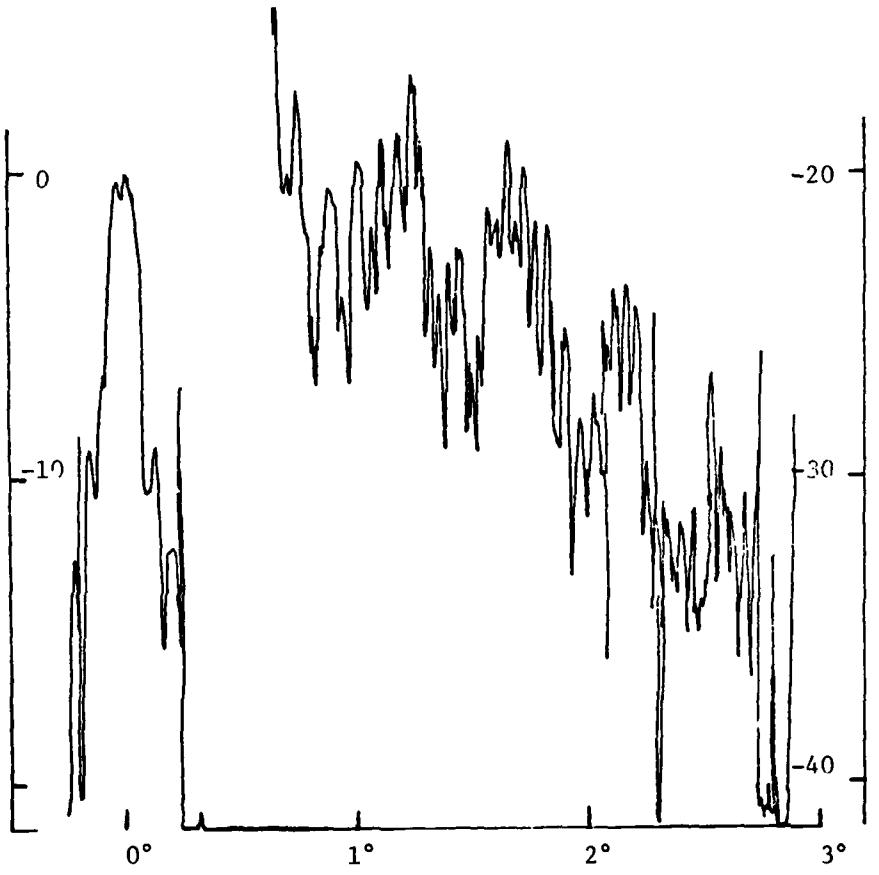

Fig. 14. In-plane scattered energy distribution of $LiNbO_3$ waveguide 88-5 with 500 V applied across a 1-mm electrode gap.

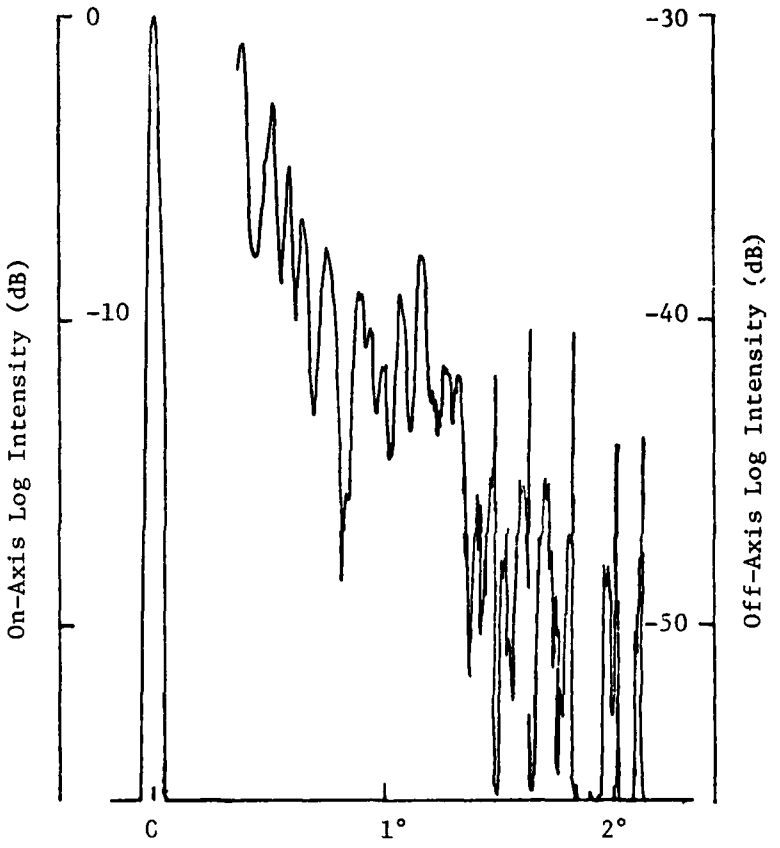

Fig. 15. In-plane scattered energy distribution of $LiNbO_3$:Ti waveguide 88-5 with 0 v applied across a 1-mm wide electrode gap.

exposure was sufficient to cause significant photorefraction. By this process negative space charge migrates to the +c side of the optical beam, leaving positive space charge at the -c side.[14] The electric field associated with this space charge produces a refractive index change by means of the electro-optic effect.

In the experiment illustrated in Fig. 16, exposure was carried out with the 515-nm beam propagating parallel to the optic axis. This direction was chosen to inhibit the formation of hologram gratings caused by the interference of scattered and unscattered components of the exposing beam. These holograms cause additional scattering that obscures the effects of interest.[15] By propagating the exposing beam parallel to the optic axis, no additional scattering was observed.

It was anticipated, however, that during exposure space charge would develop on either pole of the microdomain scattering centers, as illustrated in Fig. 16. When the waveguide is subsequently interrogated using a beam propagating perpendicular to the optic axis, the index change produced by the space charge should result in additional scattering. The extent of additional scattering is expected to be on the order of that produced by applied fields approaching 100 V/mm, since it is known that space-charge fields of that magnitude are common using photorefraction.[14] We therefore expected to see an additional scattering comparable to that observed in Fig. 14. However, no discernible change in scattering resulted.

It appears that the scattering centers are electrooptically different but photorefractively similar to the host crystal, if this null result is to be explained. This is damaging to the microdomain hypothesis. The hypothesis could be salvaged, however, if it were found that the space charge decayed during the 10 to 20 minutes that elapsed between exposure and interrogation. This is not seen to be likely, in view of the fact that space-charge holograms recorded in $LiNbO_3$ samples seldom decay this rapidly. Moreover additional scattering was not observed during exposure as might have been expected if there were a significant space-charge build up, even a temporary one.

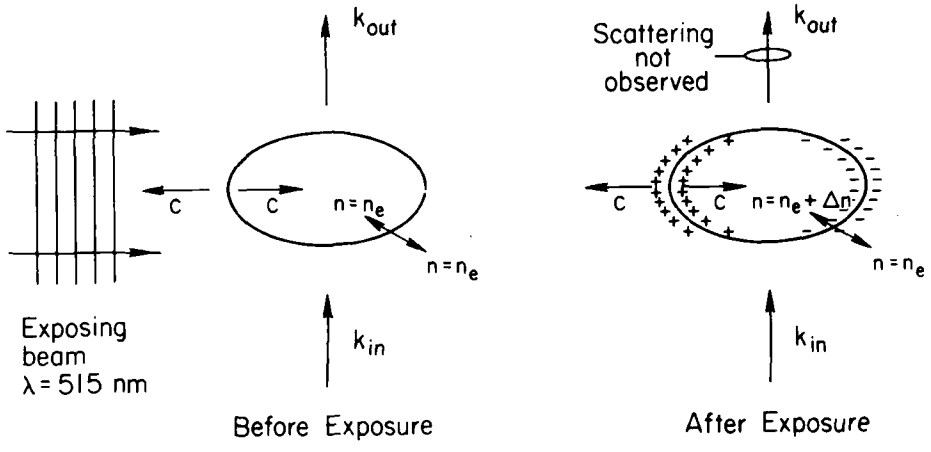

Fig. 16. Photorefractive Test of the Microdomain Model

Other Electrical Scattering Experiments in $LiNbO_3$

We perceive the electric-field dependence of scattering to be potentially useful as a means for identifying the source of residual scattering in $LiNbO_3$, despite the above described set back to the microdomain hypothesis. Accordingly we performed several other experiments of an electrical nature with the hope of understanding the mechanism at work. The first experiment was an attempt to see the electrically induced scattering using Nomarski microscopy. This was unsuccessful, even after we modified our Zeiss instrument for use with transmitted light. The reason is to be found in the small refractive-index change ($\simeq 10^{-4}$) and in the small path length ($\simeq 1\,\mu m$) over which the phase perturbation must accumulate when viewed normal to the waveguide surface.

Then we examined scattering in a bulk sample of $LiNbO_3$ about 3-mm thick and 2.3 mm wide. This enabled us to avoid waveguide mode effects and fringing-field effects associated with surface electrodes. We measured scattering at 522 V/mm and 0 V/mm and observed no difference. Later we subjected the sample to an anneal treatment at 950°C with the idea that scattering centers might be generated at the high temperatures employed for waveguide fabrication. Yet, we continued to observe no voltage induced scattering in this sample.

Next, we subjected the sample to an 1.5 h anneal at 1140°C to purposely introduce microdomains by exceeding or at least approaching the Curie temperature. As a result of the heat treatment the sample acquired a frosted appearance, indicating that we achieved our goal. We attempted to see electric-field effects in the sample using Nomarski microscopy. Again we met with no success, despite the apparent proliferation of microdomains. Then we observed scattering in the sample both with and without an applied voltage of 522 V/mm. In either case scattering was severe. However, no voltage-dependent perturbation of background scattering was observed.

A final attempt to test the microdomain hypothesis involved the exposure of an out-diffused waveguide to an intense beam of 515 nm radiation. The sample was photorefractively damaged with the idea of generating surface charge localized near scattering centers. Then the surface was viewed with an SEM in the hope of seeing the effects of surface fields on beam deflection.

In this experiment, the sample was not gold-coated since this would have shorted the electric fields of interest. Unfortunately but not surprisingly, the SEM beam itself generated surface space charge that obscured any interesting effects. The space charge accumulated preferentially over certain regions of the crystal surface, probably in response to spatial variations in cleanliness. The photograph of Fig. 17 resulted. The background speckle pattern could possibly be associated with waveguide scattering centers; however, the position of the individual speckles changed with each new raster scan of the electron beam, indicating otherwise.

Our results suggest that the voltage-dependent scattering in Ti:$LiNbO_3$ waveguides is associated with Ti-diffusion, and not with the high temperatures of fabrication. They also reinforce the conclusion to which we were drawn by our first photorefractive experiment, described earlier: microdomains are not the source of the electric-field dependent scattering in Ti:$LiNbO_3$ waveguides. Unfortunately, the experiments have not been sufficiently informative to suggest other mechanisms for the observed effect. Nor have they been sufficiently complete to definitely rule out the possibility of microdomain contributions to scattering. Other interpretations of our present results could come to the forefront in the future and make necessary the resurrection of microdomains as a scattering mechanism. However, this remains to be seen.

Ti-FREE REGIONS AND SCATTERING CENTERS ASSOCIATED WITH SAMPLE CLEANLINESS

Owing to imperfect sample cleaning and the inevitable accumulation of surface dust prior to evaporation of the Ti film used to make a waveguide, it is likely that certain regions of the film will be destroyed during the high temperature waveguide-fabrication process. This results in Ti-free regions of the waveguide having an index lower than that of the diffused regions, and therefore able to scatter light.

Ignoring the complications introduced by Li_2O outdiffusion during waveguide fabrication,[16] the index perturbation associated with the Ti-free region is $-\Delta n_e$ or $-\Delta n_o$, where $\Delta n_e(\Delta n_o)$ is the index change produced in the crystal as a whole for extraordinary (ordinary) polarized light. The

Fig. 17. SEM micrograph of an unmetallized $LiNbO_3$ surface (70X magnification).

expectation that Δn_e is typically 50% larger than Δn_o [11] is consistent with the trend to lower scattering levels for ordinary waves, seen in Figs. 10 and 11, but not consistent with the magnitude of the observed difference in scattering between ordinary and extraordinary waves.

Figure 18 shows a Nomarski micrograph of an edge of the waveguide used to obtain the data of Figs. 5 and 6. The artifacts presumably result from poor cleanliness at the sample edge. The center of the waveguide is virtually defect free. The micrograph reveals circular structures of 5-10 μm diameter that could be areas where the Ti-film exploded away at the high temperature. The structures could then correspond to Ti-free regions. Also noted are smaller, reflective structures which could correspond to regions where, for unknown reasons, Ti was not exploded away, yet was not diffused into the surface.

A theoretical indication of the potential of Ti-free waveguide regions for scattering is afforded by the theoretical analysis of Sec. II. The relevant formula is obtained from Eqs. (45) and (21):

$$\Delta P/P_{max} \simeq 4(L/W)\delta n^2 \Sigma a^2/\phi^2 \quad , \tag{47}$$

where, in the notation of Sec. II, $\Delta P/P_{max}$ is the extent of scatter reduction measured at an external scattering angle ϕ, assumed large in comparison to $\lambda_o/2\pi a$; Σ is the number density of the Ti-free regions, and δn is their average refractive index change; L is the length of the scattering medium, and W is the optical beam width. In our best waveguides we find $\Delta P/P_{max} = 10^{-4}$ (i.e., -40 dB) at $\phi = 1/60$, when L = 18 mm and W = 1.5 mm. Thus we find

$$10^{-9} \simeq \delta n^2 \Sigma a^2 \tag{48}$$

Taking a = 10 μm and ρ = 10 mm^{-2} (for a reasonably clean surface by the standards of the program) we find $\delta n \simeq 0.003$. This is comparable to the index change associated with Ti-diffusion in $LiNbO_3$, so indeed the mechanism appears capable of causing the observed levels of residual scattering in this material.

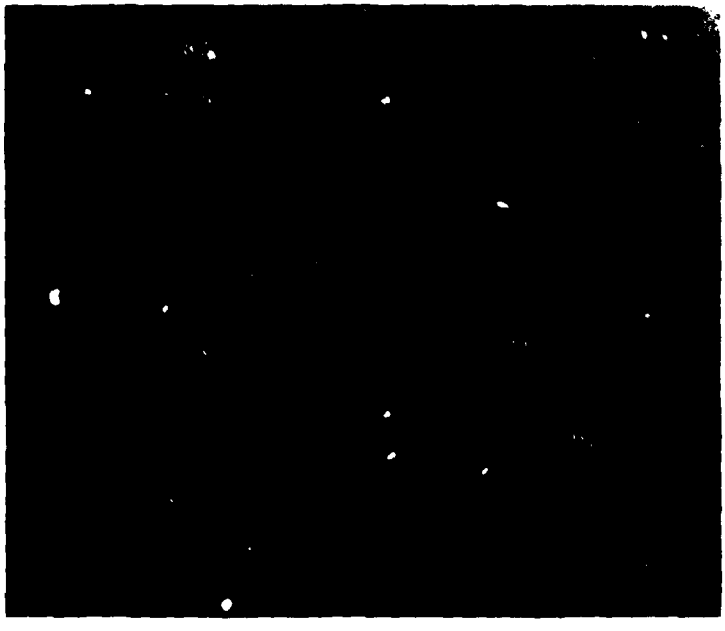

Fig. 18. Nomarski micrograph showing artifacts near the edge of a Ti-diffused $LiNbO_3$ waveguide. (500X)

$LiNbO_3 \rightarrow LiNb_3O_8$ PHASE TRANSFORMATION AS A SCATTERING MECHANISM

It is known that $LiNbO_3$ becomes unstable in the vicinity of 850°C,[12] tending to form $LiNb_3O_8$ according to the reaction

$$3LiNbO_3 \rightarrow Li_2O + LiNb_3O_8 \quad .$$

The latter compound is a monoclinic crystal having the three refractive indices 2.28, 2.36, and 2.40. Islands of this material formed during waveguide fabrication could be very efficient scatterers of light, owing to the significant deviation of the refractive indices from the 2.2 and 2.3 values of $LiNbO_3$. These scatterers are naturally anisotropic and would also be likely to display electric-field dependent scattering effects. However these effects would very likely be small in comparison to the base scattering level associated with the zero-field refractive index changes. This would be in contrast to what we have actually observed.

Diffused waveguides in $LiNbO_3$ are usually formed at temperatures of 950°C or higher. While phase transformation is not expected to be a problem at these temperatures, heating and cooling of the crystal through the 750-850°C region could produce sufficient quantities of $LiNb_3O_8$ to cause observable scattering. To test this hypothesis, a substrate of $LiNbO_3$ was heated in flowing O_2 at 850°C for 10 min. The sample was brought into the hot zone from a temperature of about 600°C, and removed to the same temperature after the heat treatment. Heating to and cooling from 850°C required several minutes each way.

The initially cleaned and polished sample was observed to have numerous pock marks and scratches following the experiment. These were conveniently observed with a Nomarski microscope under a power of 500X (Fig. 19). The scratch marks ran predominantly perpendicular to the c-axis and parallel to the direction in which the crystal was wiped during cleaning. They could, therefore, reflect strains introduced during cleaning and polishing, along which phase transformation preferentially occurred. The pock marks occurred in apparent random locations and seem to be the result of an explosive removal of material from the surface.

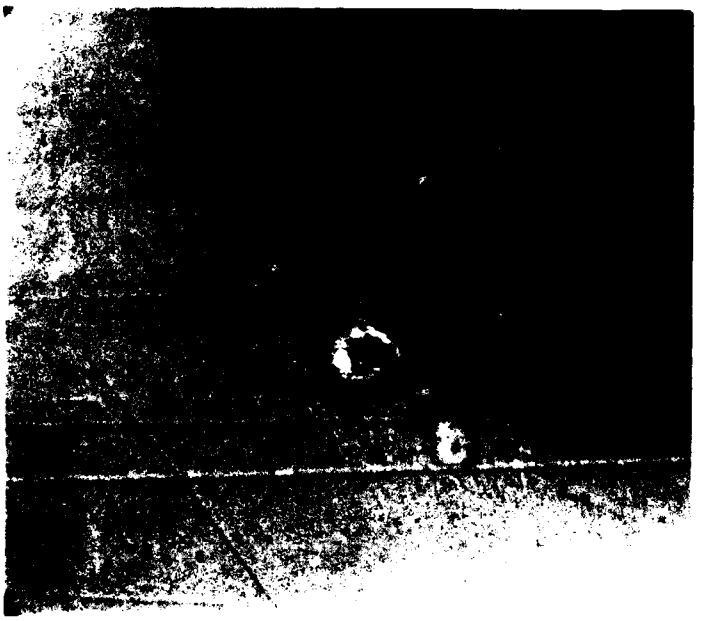

Fig. 19. Nomarski micrograph showing the results of a 10 min heat treatment of $LiNbO_3$ at 850°C in flowing O_2. (500X)

Following this experiment we examined an outdiffused $LiNbO_3$ waveguide that was made previously and known to be of good quality. This waveguide was rapidly quenched from a temperature of above 950°C to about 600-700°C as part of its fabrication. The length of time spent in the range 750-850°C is not known; however, it was as short as conveniently possible without risking fracture of the sample owing to an overly rapid quench. Under Nomarski observation the waveguide surface showed none of the scratches and pockmarks observed in Fig. 19. Consequently, the problems seen there are not characteristic of good waveguides of $LiNbO_3$. However, an incipient stage of these problems is likely to be present and may possibly be causing observed scattering levels in $LiNbO_3$.

Note added during preparation of final draft: In recent experiments we have reexamined the electric-field dependence of scattering using electrode gaps of 2 and 3 mm, as well as 1 mm. We find that the observed electric-field effects vanish as the gap becomes wider than the waveguided beam. This leads us to believe that the observed effects result from electric-field nonuniformities in the beam region, and not from the presence of electrooptic scattering centers. The absence of such centers is consistent with results obtained in photorefractive and in other electric-field experiments described in this section.

VI. DEPENDENCE OF SCATTERING ON OPTICAL WAVELENGTH, DIFFUSION TREATMENT, WAVEGUIDE VARIETY, AND WAVEGUIDE SUPERSTRATE

Owing to the investigative nature of this program, a number of avenues of experimentation were briefly explored and later terminated or assigned to lower priority status. Although these avenues were not followed to completion, they provided a number of interesting results that deserve to be reported for their potential impact on future research in the area of optical waveguide scattering reduction. This is the task of the present section. The work to be described includes interesting experiments to evaluate the dependence of scattering on wavelength, diffusion heat treatment, and waveguide superstrate. We include a discussion of the nature of waveguides formed in $LiNbO_3$ using a low temperature process employing Ag-ion exchange, and a discussion of observations made using Nb_2O_5-glass waveguides provided by the Air Force.

DEPENDENCE OF IN-PLANE SCATTERING ON WAVELENGTH

The wavelength dependence of in-plane scattering during this program was measured at 488 nm, 515 nm and 633 nm. In addition semi-quantitative observations were made at 1.06 μm. Most detailed measurements were made using a waveguide formed by diffusing a 720 Å Ti film in flowing O_2 at 1050°C for 6 h. Subsequently, the waveguide performance was improved (but not optimized) by 4 h polishing. In all likelihood, a major source of scattering in this waveguide is Li-Ti-O compound surface contamination that has not been totally removed by polishing.

Figures 20 and 21 show the in-plane scattered energy distribution of sample 88-4 at 633 nm and 515 nm respectively. A comparison of the two results shows that scattering at the shorter wavelength is approximately 6 dB worse throughout the angular range examined. This indicates a λ^{-6} variation, a variation that is in contrast to any that may be predicated on the basis of the theory presented in Sec. II. According to that theory, the wavelength dependence at small angles is either λ^{-1} for surface scattering or λ^{-3} for volume scattering. This would correspond to a 0.9 dB increase in scattering in going from 633 nm to 515 nm, if surface effects dominate, or a 2.7 dB increase

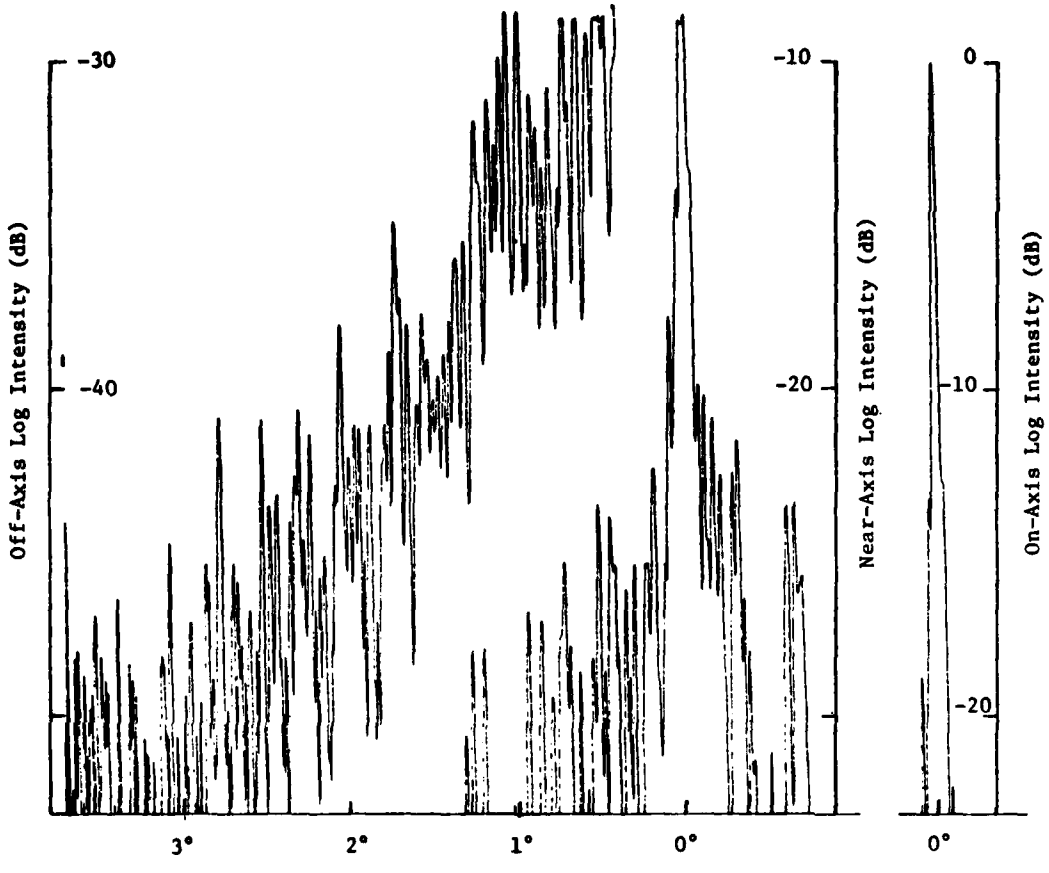

Fig. 20. In-plane scattered energy distribution of $LiNbO_3$:Ti waveguide 88-4 measured at the wavelength 0.633 μm.

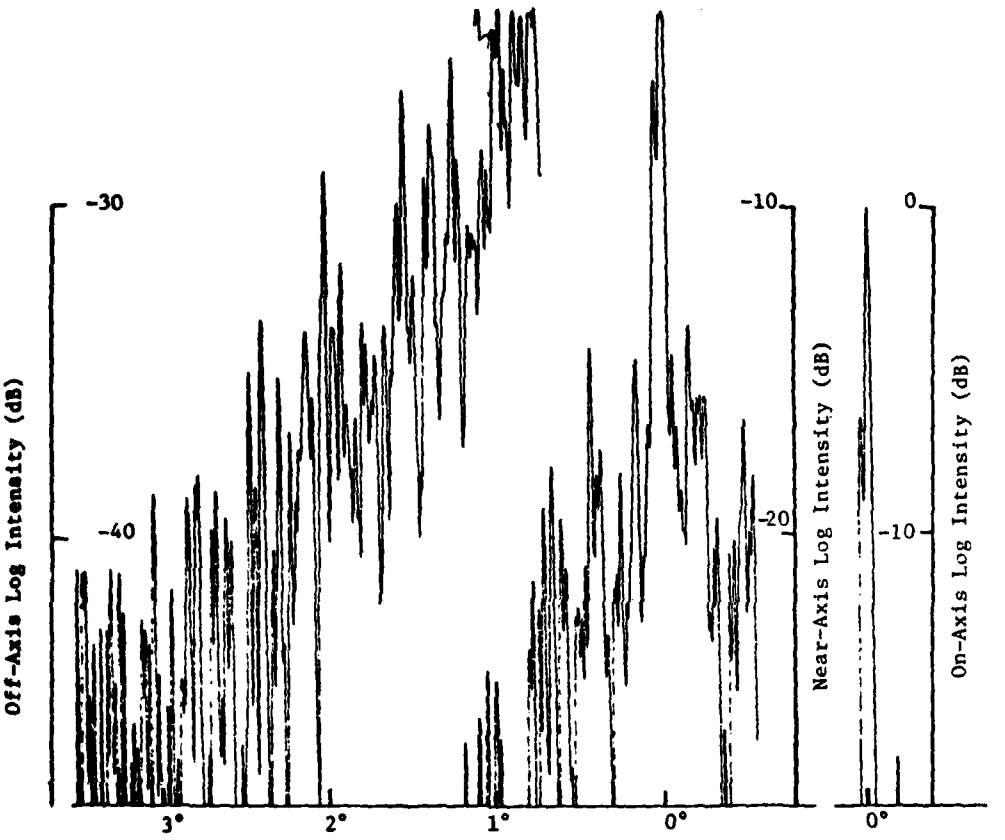

Fig. 21. In-plane scattered energy distribution of $LiNbO_3$:Ti waveguide 88-4 measured at the wavelength 0.515 μm.

in scattering if volume effects dominate. The latter value is within 3.3 dB of what we actually observe. Later in the program we noted that the background scattering level in a waveguide could change by about 3 dB depending on experimental conditions, so perhaps our results can be judged consistent with theory if volume scattering is assumed. However, our theory also states that the wavelength dependence of scattering changes by a factor λ^2 at angles ϕ for which $2\pi\eta a/\lambda >> 1$, where a is the size of the scattering center. For volume scattering the wavelength dependence changes from λ^{-3} to λ^{-1}, and the increase in scattering in going from 633 to 515 nm wavelength should only be 0.9 dB, in contrast to 6 dB observed.

To further complicate matters we found that the in-plane scattered energy distribution measured at 488 nm was very similar to that at 515 nm. If anything, scattering was reduced in going to the shorter wavelength. According to the measured λ^{-6} dependence, the scattering level should have increased by 1.4 dB.

These results are not supportive of the theory developed in Sec. II, but before that theory is modified it is necessary to take more numerous and more careful data in the wavelength dependence of scattering than we did in the program. As an example of the care required, we note that the scattering associated with prism coupling may well be λ-dependent. This possibility has not been considered in our interpretation of the data of Fig. 20 and 21. Moreover these data could have been influenced by an experimental problem that resulted in spurious scattering distributions for a period of time during this program.

DEPENDENCE OF IN-PLANE SCATTERING ON DIFFUSION HEAT-TREATMENT

In Fig. 7 we presented the results of a study that showed the influence of Ti-film thickness on the scattering characteristics of Ti:$LiNbO_3$ waveguides. These results motivate the question as to whether, for constant Ti-film thickness, waveguide quality depends on diffusion time, temperature, or crystal orientation. Our results based on a few waveguide samples indicate that this is not the case:

Item 1. Sample 88-5 (see Figs. 14 and 15), made by diffusing 280 Å of Ti for 3 h at 950°C, and subsequently polished for 1 h, was given an additional 3 h heat treatment. There was no significant change in the in-plane scattered-energy distribution as a result.

Item 2. y-cut sample 109 (see Figs. 5 and 6) exhibited scattering characteristics similar to those of x-cut sample 88-5. Both waveguides were made under similar diffusion conditions.

Item 3. Sample 88-3, made by diffusing 720 Å of Ti for 8.5 h at 950°C, exhibited scattering characteristics similar to those of sample 88-4 (Figs. 20 and 21) made by diffusing 720 Å of Ti for 6 h at 1050°C. For the comparison, neither sample was polished. Both samples were x-cut and performed similarly to y-cut sample 70, which was comparable to 88-3 and 4 except for a shorter 3 h diffusion time. (Various results for sample 70 are displayed in Figs. 7, 10, 11 and 12).

These items indicate that waveguide scattering performance is relatively insensitive to the time and temperature of the diffusion treatment and to the crystal orientation (x-cut or y-cut) of the $LiNbO_3$ surface. Accordingly, we did not devote much effort to categorizing the small dependences on these conditions that may exist.

However, at one point in the program we were concerned about the possibility that the high temperatures of diffusion could introduce scattering centers that might be avoided through the use of a low-temperature diffusion process. In an attempt to check this out we fabricated and tested an Ag:$LiNbO_3$ waveguide. Our first attempt to make the waveguide involved the thermal diffusion of Ag-films at temperatures up to 450°C for times up to 14 h. In x-cut sample 105, the film appeared to be partially diffused. Residue was nonuniformly distributed across the substrate surface. No waveguiding was observed, even after the residue was lightly polished.

We finally were successful in making the desired waveguide using Ag-Li ion-exchange in a bath of molten $AgNO_3$.[17] The exchange took place at a temperature of 360°C for a time of 6.5 h. The waveguide exhibited a single TE_o mode, and that was for the case of propagation perpendicular to the optic axis.

The surface of the waveguide was strongly degraded by the fabrication process. It was improved but not restored by a three hour polishing treatment. A 500X Nomarski micrograph of a typical portion of the polished surface is shown in Fig. 22.

The waveguide appeared to be quite lossy; however it was difficult to evaluate the losses visually because of poor input- and output-coupling

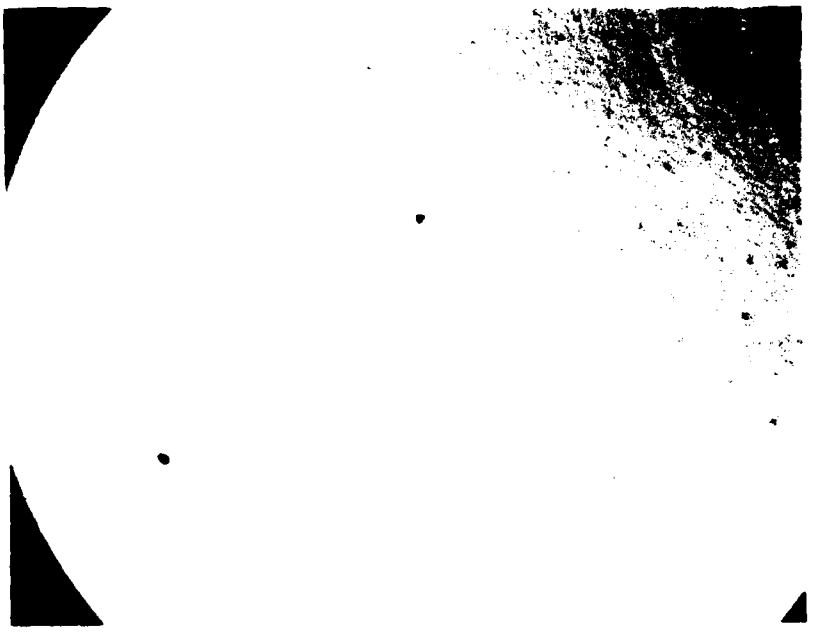

Fig. 22. Nomarski micrograph of the surface of an Ag:$LiNbO_3$ waveguide formed by ion-exchange (500X).

efficiency. The sample had a slightly brownish cast, and it is possible that much of the loss was from absorption rather than scattering. This was further indicated by the surprising result that the scattered energy distribution of the Ag:$LiNbO_3$ waveguide, shown in Fig. 23 was only slightly inferior to those of good Ti:$LiNbO_3$ waveguides. This result shows an insensitivity of in-plane scattering to surface condition that was, to us, entirely unexpected on the basis of beliefs we held at the start of the program.

DEPENDENCE OF IN-PLANE SCATTERING ON WAVEGUIDE SUPERSTRATE

In the theory of optical-waveguide scattering presented in Sec. II, a number of formulas were derived which showed a dependence on the superstrate refractive index. These formulas do not include those of Eq. (28) for the in-plane differential scattering cross section. Consequently, we expect the in-plane scattered energy distribution to remain unchanged when the waveguide superstrate is changed, as may be done by adding a liquid to the waveguide surface. We verified experimentally that this was the case, using a liquid having $n_o = 1.544$, obtained from a set of index-matching liquids.

Among the formulas derived in Sec. II which do depend on the superstrate index are Eq. (37) for the out-of-plane differential scattering cross section and Eq. (40) for the waveguide attenuation. Assuming that either surface or volume scattering makes the dominant contribution to total out-of-plane scattering, we may write

$$\alpha = K(n_1^2 - n_o^2)^m \tag{49}$$

where α is the attenuation coefficient, K is a constant that depends on scattering and waveguide parameters, n_1 is the waveguide index, n_o is the superstrate index, and $m = +0$ for surface scattering or $m = -3$ for volume scattering.

The quantity $P = P_o e^{-\alpha L}$ is the power transmitted through a length L of waveguide when P_o is the initial power. The change in transmitted power that results when α is changed is an experimentally accessible quantity. In particular,

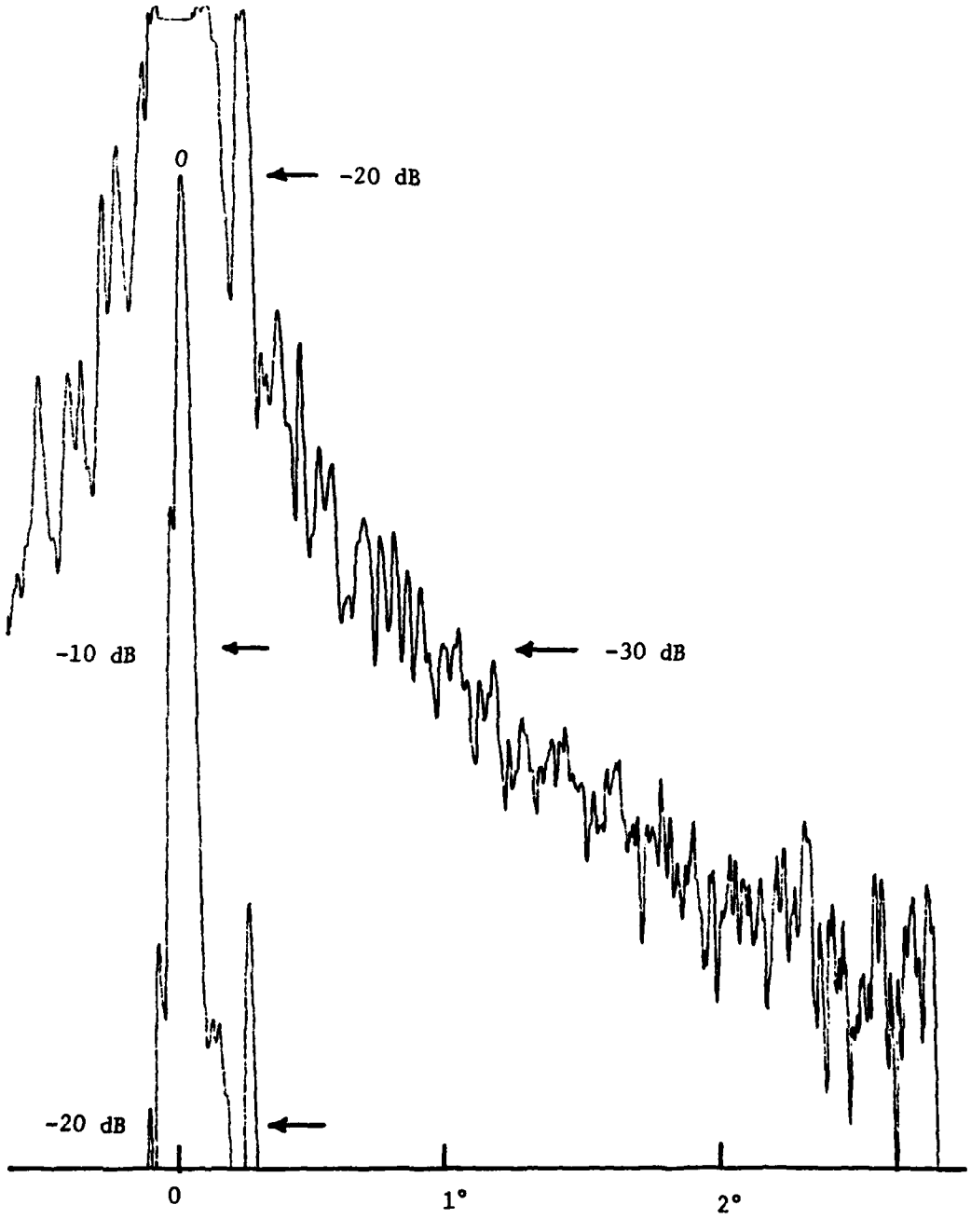

Fig. 23. In-plane scattered energy distribution of an Ag:$LiNbO_3$ waveguide formed by ion exchange.

$$\Delta P/P = e^{(\alpha_D - \alpha_W)L} - 1 \tag{50}$$

is the fractional change in transmitted power that occurs when a liquid is added to the waveguide surface, where α_W is the attenuation coefficient for a wet surface, and α_D, is the attenuation for a dry surface ($n_o = 1$). For low loss waveguides,

$$\Delta P/P \simeq \alpha_D L(1 - \alpha_W/\alpha_D) \tag{51}$$

where, using Eq. 49,

$$\alpha_W/\alpha_D = [(n_1^2 - n_o^2)/(n_1^2 - 1)]^m \quad , \tag{52}$$

For the values $n_1 = 2.2$ and $n_o = 1.544$, we find

$$(\Delta P/P)_{surf} = 0 \tag{53}$$

$$(\Delta P/P)_{vol} = -2.82\ \alpha_D L$$

for surface and volume scattering, respectively.

We have measured $\Delta P/P$ for Ti:$LiNbo_3$ waveguide sample 88-3 and for Ag:$LiNbO_3$ waveguide sample 105. Both waveguides exhibited approximately 30 dB scatter reduction at 1°, but the latter had a much inferior surface quality, as shown in Fig. 22. For the Ti:$LiNbO_3$ waveguide we find $\Delta P/P \simeq + 0.0105 \pm 0.0078$, while for the Ag:$LiNbO_3$ waveguide our measurement yielded $\Delta P/P \simeq 0.1148 \pm 0.0088$.

The fact that positive values are obtained suggests that surface roughness is the dominant out-of-plane scattering mechanism. However, the theory of Section II is not adequate to predict these values. This may be owing to several simplifying approximations used in the development of that theory. A useful set of measurements would be one in which $\Delta P/P$ is measured

for a range of superstrate indices n_o, so that the functional dependence of α on n_o could be accurately tested. Possibly, this technique could be helpful in assessing the relative amounts of surface roughness and volume scattering.

IN-PLANE SCATTERING CHARACTERISTICS OF AN Nb_2O_5-GLASS WAVEGUIDE

Alternatives to Ti:$LiNbO_3$ waveguides that are candidates for use in the spectrum-analyzer application[1] are waveguides formed by sputtering glass or metal oxides on thermally oxidized Si substrates. We report briefly here on observations we made on an Nb_2O_5-microscope-slide waveguide that was provided us by Dr. Douglas Wille of the Air Force Avionics Lab.

The in-plane scattered-energy distribution for this waveguide is shown in Fig. 24. The asymmetry in the angular distribution is believed to result from a geometric asymmetry in our detection system that we were experiencing at the time this graph was generated. Consequently, repeat data should be acquired before final evaluation of this waveguide relative to $LiNbO_3$ waveguides tested in the program. Our tentative conclusion is that the two types are comparable with regard to the initial rate of fall-off of scattered intensity with angle. However, the total angular span of the visible in-line was much greater in the Nb_2O_5-glass waveguide than in a typical Ti:$LiNbO_3$ waveguide. The longer m-line would be expected to result from the presence of a background distribution of particles small in size compared with a wavelength. The apparent absence of such a distribution in $LiNbO_3$ waveguides is an attractive feature of this material.

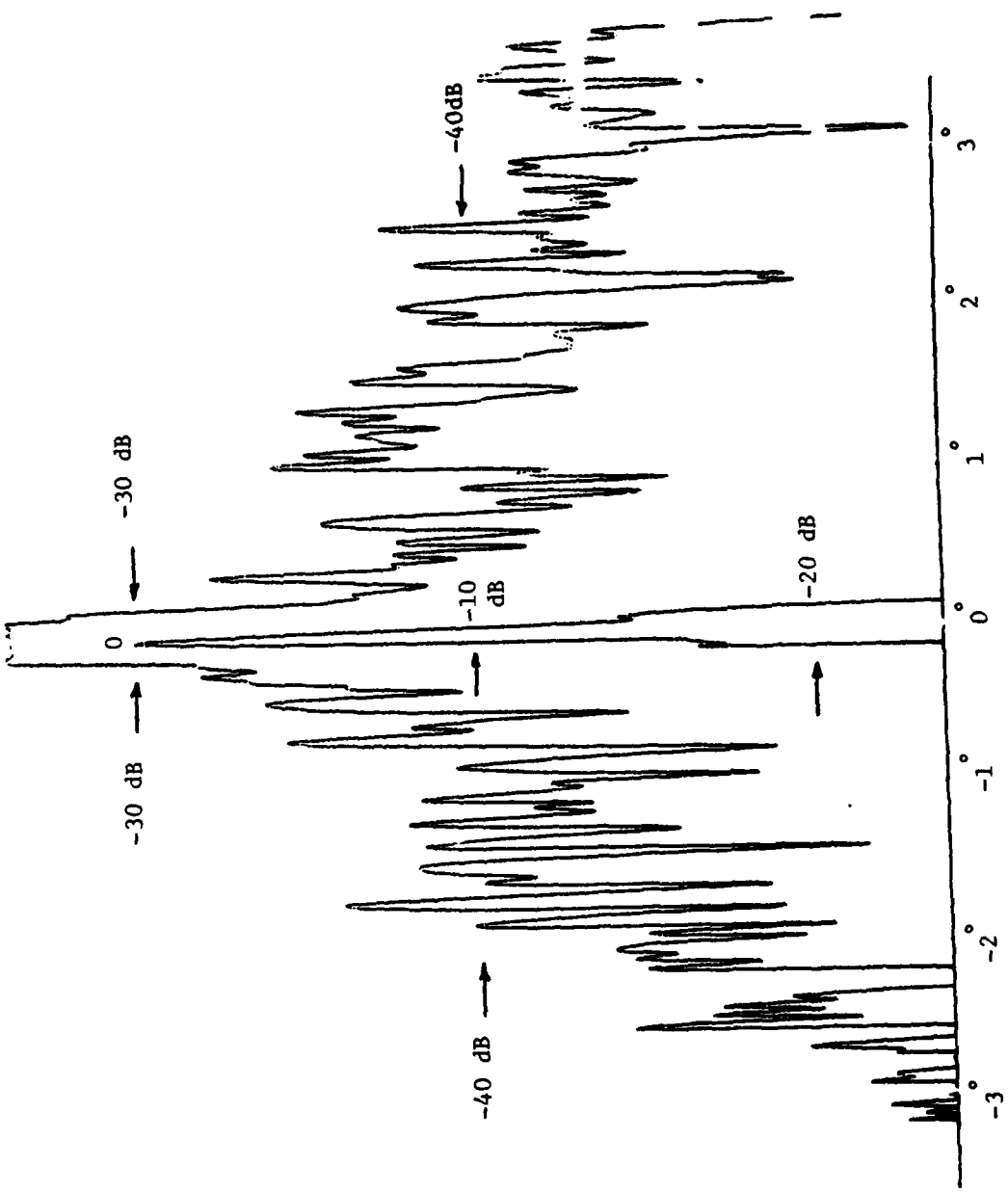

Fig. 24. In-plane scattered-energy distribution of an Nb_2O_5 —glass waveguide.

REFERENCES

1. M. C. Hamilton, D. A. Wille, and W. J. Miceli, "An Integrated Optical RF Spectrum Analyzer", Optical Engineering, 16 (5), 475-478 (1977).

2. D. W. Vahey, C. M. Verber and R. P. Kenan, "Development of an Integrated Optics Multichannel Data Processor" in Guided Wave Optical Systems and Devices, SPIE, Vol. 139, 151-158 (1978).

3. D. Marcuse, Light Transmission Optics, Van Nostrand Reinhold, New York, 1972, Chapters 8 and 9.

4. J. T. Boyd, and D. B. Anderson, "Effect of Waveguide Optical Scattering on the Integrated Optical Spectrum Analyzer Dynamic Range", IEEE J. Quantum Electron, Vol. QE-14, No. 6, 437-443 (1978).

5. T. G. Giallorenzi, "Acousto-Optical Deflection in Thin-Film Waveguides", J. Appl. Phys., 44 (1), 242-253 (1973).

6. D. J. Walter and J. Houghton, "Attenuation in Thin Film Optical Waveguides Due to Roughness Induced Mode Coupling", Thin Solid Films, 52, 461-476 (1978).

7. H. Mori and M. Itakura, "The Scattering Centers in Dielectric Thin-Film Optical Waveguides", Japan J. Appl. Phys., 14 (12), 1917-1924 (1975).

8. K. H. Haegele and R. Ulrich, "Pyroelectric Loss Measurement in $LiNbO_3$:Ti Guides", Opt. Lett., 4 (2), 60-62 (1979).

9. B. Chen and M. K. Barnowski, "Design, Fabrication and Integration of Components for the Integrated Optical Spectrum Analyzer", Talk 176-11, SPIE Technical Symposium East, April 17-20, 1979, Washington, D.C.

10. T. P. Pearsall, S. Chiang, and R. V. Schmidt, "Study of Titanium Diffusion in Lithium-Niobate Low-Loss Optical Waveguides by X-ray Photoelectron Spectroscopy", J. Appl. Phys., 47 (11), 4794-4797 (1976).

11. W. K. Burns, P. H. Klein, E. J. West, and L. E. Plew, "Ti Diffusion in Ti:$LiNbO_3$ Planar and Channel Optical Waveguides", to be published.

12. L. O. Svaasand, M. Eriksrud, G. Nakken, and A. P. Grande, "Solid Solution Range of $LiNbO_3$", J. Crystal Growth, 22, 230-232 (1974).

13. N. Ohnishi, "An Etching Study on a Heat-Induced Layer at the Positive Domain Surface of $LiNbO_3$", Japan J. Appl. Phys., 16 (6), 1069-1070 (1977).

14. A. M. Glass, "The Photorefractive Effect", Opt. Engineering, 17 (5), 470-479 (1978).

15. R. Magnusson and T. K. Gaylord, "Laser Scattering Induced Holograms in Lithium Niobate", Appl. Opt. 13 (7), 1545-1548 (1974).

16. B. U. Chen, and A. C. Pastor, "Elimination of Li_2O Outdiffusion Waveguide in $LiNbO_3$ and $LiTaO_3$", Appl. Phys. Lett., 30 (11), 570-571 (1977).

17. Manhar L. Shah, "Optical Waveguides in $LiNbO_3$ by Ion Exchange Technique", Appl. Phys. Lett., 26 (11), 652-653 (1975).

18. D. Marcuse, Theory of Dielectric Optical Waveguides, Academic Press, New York, 1974, Chapter 1.

19. D. Marcuse, "Mode Conversion Caused by Surface Imperfections of a Dielectric Slab Waveguide", Bell Syst. Tech. J., 48 (10), 3187-3215 (1969).

*U.S.Government Printing Office: 1980 — 657-084/521